ISSN 0869-5938, Stratigraphy and Geological Correlation, 2024, Vol. 32, No. 4, pp. 374–395. © Pleiades Publishing, Ltd., 2024.

High-K Rocks of the Late Riphean Mara Paleovolcano, Biryusa Uplift, South of the Siberian Platform

A. E. Izokh[a, *], E. F. Letnikova[a], I. A. Izbrodin[a], A. V. Ivanov[a], S. I. Shkolnik[a, b], and A. G. Doroshkevich[a]

[a] *Sobolev Institute of Geology and Mineralogy, Siberian Branch, Russian Academy of Sciences, Novosibirsk, 630090 Russia*
[b] *Institute of the Earth's Crust, Siberian Branch, Russian Academy of Sciences, Irkutsk, 664033 Russia*
**e-mail: izokh@igm.nsc.ru*

Received July 4, 2023; revised September 5, 2023; accepted October 9, 2023

Abstract—The studies are focused in the Mara–Kamenka–Uvat interfluve of the Biryusa Uplift of the basement of the Siberian Platform, where the Mara paleovolcano was recognized during the prospecting works for manganese more than 50 years ago. The specific volcano-sedimentary rocks are considered in the structure of the Late Riphean Karagas Group. Our mineralogical and petrographic studies allowed us to establish abundant high-K pyroclastic rocks, ignimbrites, and trachybasalts, which indicate a subaerial explosive character of the Mara volcano. The age of high-K volcanism of 640 Ma is based on U–Th–Pb dating of zircon. The Lu–Hf isotope systematics of zircon indicates a link of volcanism with mantle magmas. The composition and the period of the formation of rocks prevent their correlation (as was considered before) with sedimentary Late Riphean quartz and quartz–feldspar sandstones of the Karagas Group and dolerites of the Nersa intrusive complex. Specific mineralogical–petrographic features of rocks allow their use as a regional stratigraphic reference.

Keywords: high-K pyroclastic rocks, Zima alkaline intrusive complex, Late Riphean, Siberian Platform
DOI: 10.1134/S0869593824700060

INTRODUCTION

Igneous complexes of Late Riphean alkaline rocks and carbonatites, which are ascribed to the Zima intrusive complex, are abundant in the Biryusa Sayan region, in the south of the Siberian Platform: the Belaya Zima (643 ± 4 and 645 ± 6 Ma; Yarmolyuk et al., 2005 and Doroshkevich et al., 2016, respectively), Zhidoi (632 ± 2 Ma; Yarmolyuk et al., 2005), and Bolshaya Taiga (644 ± 9 Ma; Savelieva et al., 2022) plutons. Egorov et al. (2010) indicated abundant Late Riphean alkaline volcanism (including high-K or lamproitic) on this territory. The Neoproterozoic rift-related magmatism in the south and southwest of the Siberian Craton is linked to a breakup of the Rodinia Supercontinent in the Late Precambrian (700–600 Ma) (Yarmolyuk et al., 2005). No products of this tectonomagmatic event have been identified in the Late Precambrian sedimentary successions of the south of the Siberian Platform to date. It was considered that the sedimentary rocks of the Biryusa Sayan region in the Neoproterozoic accumulated in shallow shelf conditions during a relatively short period of time (Metelkin, 2012). The Late Precambrian sections, which mainly include the rocks of the Karagas Group, contain ubiquitous dolerites of the Nersa complex with the age of 787–718 Ma (Gladkochub et al., 2012; Romanova et al., 2012), which limits the upper boundary of the sedimentation of this group.

The traditional provenances of clastic material to the sedimentary basins of the Siberian Platform include the rocks of its Early Precambrian basement, as well as igneous and volcanic rocks related to different stages of its tectonomagnatic activation. Their erosion resulted in the accumulation of sediments with dominant quartz clasts. The Late Precambrian sedimentary successions in the southern part of the platform contain clastic rocks with dominant K-feldspar at a subordinate amount of quartz and plagioclase. They are characterized by high K_2O (5–14 wt %) and low Na_2O contents (Table 1). The high-K rocks have no contacts with sedimentary rocks of the Karagas Group in any of the studied outcrops, whereas they represent individual often extended isolated fragments of red successions. They exhibit the intercalation of clastic small- to coarse-grained rocks with massive to bedded textures. There are ubiquitous gravel conglobreccias with clasts of altered volcanic rocks. The high-K rocks strongly differ in petrographic, mineral, and geochemical composition from quartz and quartz–two-feldspar terrigenous rocks of the Karagas Group, the rocks of possible provenances of metamorphic rocks of the basement of the Biryusa Block (Subluk Formation), and granites of the Sayan complex, but they have similar geochemical characteristics with alkaline igneous rocks of the Late Riphean Zima complex (Letnikova et al., 2012). This feature has long been ignored.

Table 1. Contents of major oxides (wt %) and trace elements and rare earth elements (ppm) of high-K rocks, Precambrian crystal schists, and granitoids of the Biryusa Uplift

Component	Sample number					
	M41/07	C38/07	A-542-81	A-543-81	K13/14	1097
SiO_2	53.97	75.38	51.97	61.71	67.37	71.97
TiO_2	0.58	0.43	0.61	0.73	0.76	0.24
Al_2O_3	10.35	11.65	14	16.24	14.7	14.15
$Fe_2O_3^*$	1.82	1.09	5.58	4.94	6.3	2.81
MnO	0.08	0.01	0.07	0.12	1.94	0.01
MgO	5.18	0.15	3.04	0.18	0.33	0.69
CaO	7.88	0.46	4.72	0.07	0.95	0.26
Na_2O	0.02	0.07	0.15	0.11	4.66	3.22
K_2O	8.24	9.54	12.01	14.11	0.09	4.83
P_2O_5	0.1	0.33	0.21	0.05	0.1	0.08
H_2O-	0.04	0.09	–	–	0.03	0.25
LOI	0.09	0.24	–	–	2.36	1.41
CO_2	11.69	0.06	–	–	–	<0.06
Total	100.04	99.5	92.36	98.26	99.59	99.92
Rb	87.92	118.56	146.84	168.01	–	290
Sr	43.29	29.11	19.33	18.47	–	60
Y	12.94	20.94	26.22	28.99	–	17
Zr	241.6	295.14	–	–	–	150
Nb	10.5	7.32	–	–	–	24
Ba	306	517.60	355.66	515.70	–	300
La	24.57	30.06	43.53	49.81	–	59.15
Ce	53.97	65.48	83.59	93.23	–	134.28
Pr	5.475	7.29	10.02	11.47	–	15.26
Nd	20.69	26.82	34.54	37.50	–	49.48
Sm	3.63	4.90	6.06	6.63	–	8.6
Eu	0.72	0.97	1.20	1.31	–	0.51
Gd	2.27	4.01	5.64	5.77	–	6.1
Tb	0.37	0.56	0.83	0.91	–	0.7
Dy	2.14	3.38	4.85	5.17	–	4.12
Ho	0.47	0.71	0.91	1.02	–	0.72
Er	1.24	1.99	2.64	2.87	–	2.03
Tm	0.18	0.31	0.40	0.43	–	0.29
Yb	1.28	2.09	2.50	2.67	–	2.09
Lu	0.22	0.30	0.34	0.37	–	0.29
Th	5.24	9.07	–	–	–	41.41
U	1.78	1.50	2.72	3.24	–	5.15

Samples M41/07, C38/07, A-542-81, and A-543-81, high-K rocks; Sample K13/14, crystalline schist of the Proterozoic Subluk Formation; Sample 01097, two-mica granite of the Biryusa pluton (Donskaya et al., 2014). Samples A-542-81, A543-81 from A.D Nojkin's collection.

The aim of this paper is to show that the high-K rocks of the Mara–Kamenka–Uvat interfluve formed as a result of explosive volcanism synchronous with alkaline magmatism of the Zima complex (640 Ma) and their correlation with the Karagas Group is unwarranted.

ANALYTICAL METHODS

The chemical composition of high-K rocks (major oxides, trace elements, and rare earth elements (REEs)) was analyzed using X-ray fluorescence and inductively coupled plasma mass spectrometry at the Center for Collective Use of Mul-

tielemental and Isotopic Studies, Siberian Branch, Russian Academy of Sciences (CCU MIS SB RAS, Novosibirsk, Russia).

Zircon for U–Th–Pb dating was extracted at the CCU MIS SB RAS following a standard method based on a combination of magnetic and heavy liquid separation. The zircon monofractions were manually picked up under a binocular microscope. The internal structure of zircon grains was studied on a JEOL JSM 6510LV scanning electron microscope (SEM) (CCU MIS SB RAS) in the cathodoluminescence regime. The U–Th–Pb age of zircon grains was measured using laser ablation inductively coupled plasma mass spectrometry (LA-ICP-MS) at the Vernadsky Institute of Geochemistry and Analytical Chemistry, Russian Academy of Sciences (Moscow, Russia), on an Element XR mass spectrometer (Thermo Finnigan) equipped with a UP-213 laser ablation system at a crater diameter of 30–40 μm. The zircon standards GJ and 91500 were used for calibration and measurement control. The method is described in detail in (Kostitsyn and Anosova, 2013). The data were processed in the Glitter program (van Achterbergh et al., 1999). The age of the crystallization of zircons older and younger than 1000 Ma in primary rock was calculated from the $^{207}Pb/^{206}Pb$ and $^{206}Pb/^{238}U$ ratios, respectively.

All studies described below were conducted at the CCU MIS SB RAS. The Raman spectra of minerals were registered on a Horiba Jobin Yvon HR800 Raman spectrometer equipped with a 1024-pixel CCD detector with a 1800-g/mm grid, an Olympus microscope (LMPLFLN 50× and 100× objectives), and a solid-state laser with a wavelength of 532 nm. The Raman shift was calibrated relative to a Si peak standard at 520.5 ± 1 cm^{-1}.

The textural–structural characteristics of rocks and the composition of minerals were studied on a Tescan MIRA 3 LMU SEM equipped with an INCA Energy 450 X-Max 80 energy-dispersive analyzer (Oxford Instruments) at an accelerating voltage of 15 kV and a beam current of 1.5 nA and with the Oxford Instruments INCA 5.05 microprobe program. The chemical composition of apatite (grains more than 10 μm) was determined on a Camebax-micro microprobe at a beam current of 20–25 nA, an accelerating voltage of 20 kV, a beam size of 2 μm, and an analytical time of each element of 10 s. Synthetic chlorapatite and natural fluorapatite were used as standards for calibration.

RESULTS OF INVESTIGATION

Our studies were focused on the Mara–Kamenka–Uvat interfluve (Figs. 1, 2), where the Mara paleovolcano located on the Uvat Uplift was recognized more than 50 years ago during prospecting works for manganese (Bessolitsyn et al., 1969). The authors of this thematic report considered that the tuff breccias of the basin of the Mara River belong to relics of caldera complexes of bimodal rift-related volcanism. The presence of a volcano in this area, in their opinion, was evident from the findings of psephitic tuffs in the basin of the Kamenka River and the ignimbrite beds of alkali porphyries. The close location of a volcanic source was indicated by inclusions of lapilli of alkali porphyries and signatures of fumarole activity (hematitization and carbonatization). Similar to the Mara paleovolcano, the Kremenshet, Biryusa-1, Biryusa-2, Izan, Slyudyanka, and Taishet paleovolcanoes were recognized from the findings of volcanic breccias in the lower part of the second member of the Shangul'ezh Formation (Fig. 1). These volcanoes erupted basaltic, trachytic, and felsic high-K lavas and tuffs with a high degree of explosion (Bessolitsyn et al., 1969). Later, however, these geological prospecting and searching materials were ignored and volcano-sedimentary rocks were forgotten and included in the sedimentary Karagas Group, whereas the trachydolerites and trachybasalts were ascribed to the Nersa intrusive complex.

In the Mara–Kamenka–Uvat interfluve, the volcano-sedimentary rocks are underlain by a thick sequence of quartz and quartz–feldspar sandstones and polymictic conglomerates, which are ascribed to the Karagas Group. The thickness of the volcano-sedimentary sequence is 100–125 m. A combined section of volcano-sedimentary rocks of the Mara–Kamenka–Uvat interfluve in the northern part of the Mara paleovolcano is shown in Fig. 3.

We studied the volcano-sedimentary rocks in a reference section of the Mara paleovolcanic field (Figs. 2, 3). The main attention was paid to the substantiation of the volcanic origin of these rocks and their composition. The studied section contains ignimbrites (Fig. 4), tuff breccias, tuffs, and tuffites, which are intercalated with sandstones and siltstones (Figs. 5a, 5c). The high-K rocks (K_2O content is 5–14 wt %) are characterized by lilac–cherry and reddish colors caused by the presence of K-feldspar and hematite. There are tuff breccias (Fig. 4a), tuff sandstones (Fig. 4b), and tuff siltstones (Fig. 4c) with weak bedding. The latter host no lithoclasts and the crystal

Fig. 1. Scheme of geological structure of the Biryusa Uplift, after (*Geologicheskaya...*, 2012). (1) Biryusa Group, PR_1; (2) Subluk Group, PR_2; (3) Sayan intrusive complex, PR_2; (4) Biryusa intrusive complex, PR_2; (5) Karagas Group, R_3; (6) Oselok Group, V; (7) Ust Tagul Group, $Є_1$; (8) Paleozoic rocks of the Siberian Platform; (9) paleovolcanoes of the Biryusa Uplift: (*1*) Biryusa-1; (*2*) Biryusa-2; (*3*) Izan; (*4*) Slyudyanka; (*5*) Taishet; (*6*) Mara; (*7*) Kremenshet. Inset shows the region of studies. Black squares, outcrops of the Late Precambrian alkaline and high-K rocks of the southwestern part of the Siberian Platform: (1) lamproites; (2–4) alkaline rocks of the Belaya Zima, Zhidoi, and Bolshaya Taiga plutons, respectively; (5, 6) ultra-K trachytes; (7) micaceous picrites (Egorov et al., 2010).

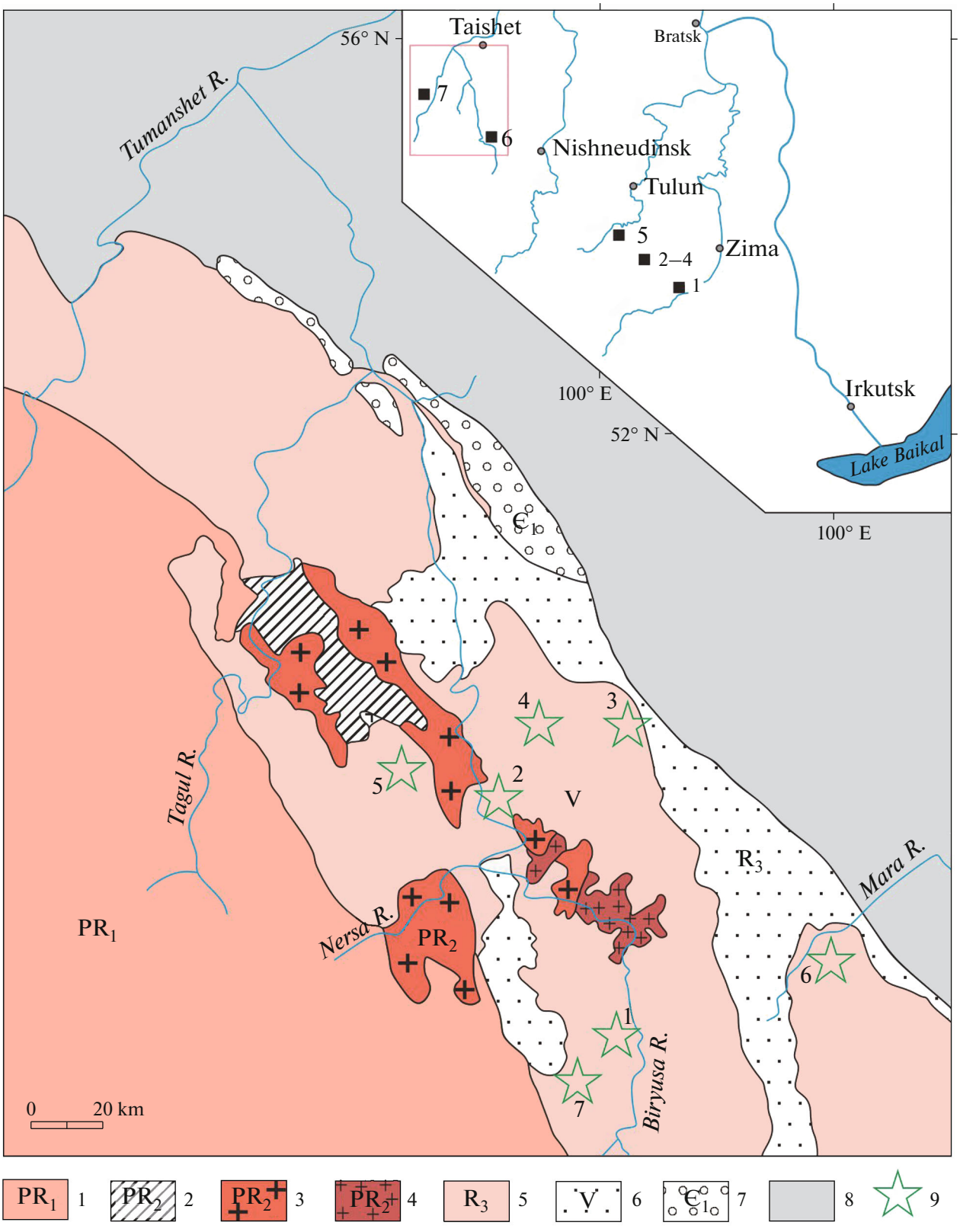
Taishet
Bratsk
56° N
Tumanshet R.
7
6
Nishneudinsk
Tulun
5
2–4
Zima
1
Irkutsk
100° E
52° N
Lake Baikal
100° E
ϵ_1
4
3
5
2
V
R_3
Mara R.
Tagul R.
PR_1
Nersa R.
PR_2
6
1
7
Biryusa R.
0 20 km
PR_1 1
PR_2 2
PR_2 3
PR_2 4
R_3 5
V 6
ϵ_1 7
8
9

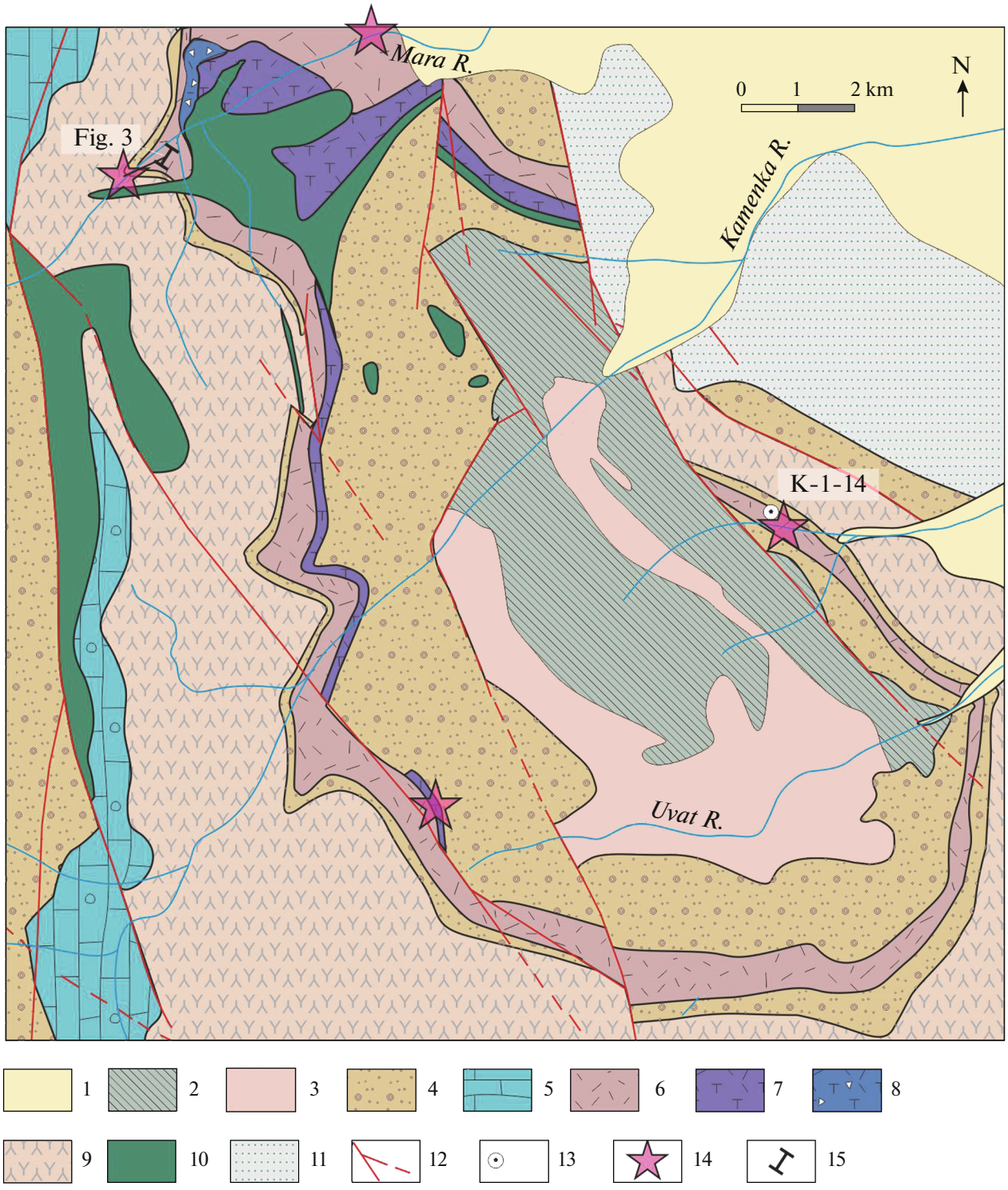

Fig. 2. Scheme of geological structure of the Mara volcanic field, simplified and modified after (Bessolitsyn et al., 1969). (1) Quaternary deposits; (2, 3) volcano-sedimentary sequences of the pre-Vendian basement: (2) sedimentary-metamorphic rocks (unspecified); (3) felsic volcanic rocks; (4, 5) Karagas Group: (4) conglomerate–sandy (continental) rocks; (5) carbonate rocks; (6) volcanic rocks of the Mara paleovolcano (unspecified); (7) alkali ignimbrites; (8) caldera (?) subsidence breccias; (9) carbonate–terrigenous–tuffaceous rocks; (10) gabbrodiabases, gabbro of the Nersa complex; (11) sedimentary rocks of the Oselok Group; (12) faults; (13) sampling place and sample number for the U–Pb isotopic-geochronological studies; (14) sampling place for mineralogical-petrographic and geochemical studies; (15) position of the combined section (Fig. 3).

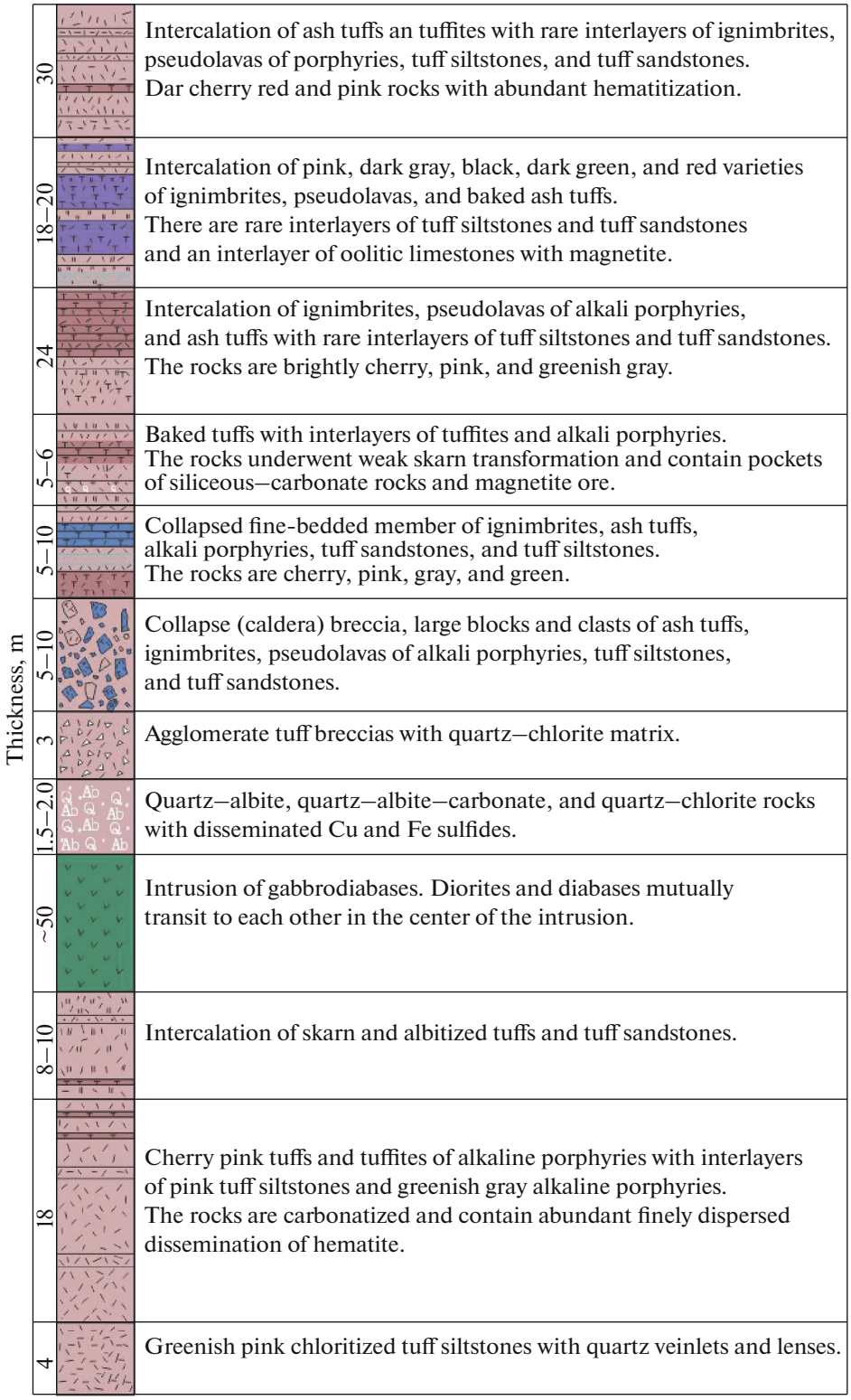

Fig. 3. Combined section of volcano-sedimentary rocks of the Mara–Kamenka interfluve, after (Bessolitsyn et al., 1969).

clasts include only K-feldspar with a higher Ba content. Other beds exhibit fine bedding caused by the intercalation of tuff sandstones, tuff siltstones, and tuffites. The fine-grained tuffites have syneresis cracks evident of on-land eruptions. The tuff interlayers are characterized by coarse sorting of the material and the presence of small lithoclasts of basalts and rhyolites. The crystal clasts include K-feldspar laths. Some sam-

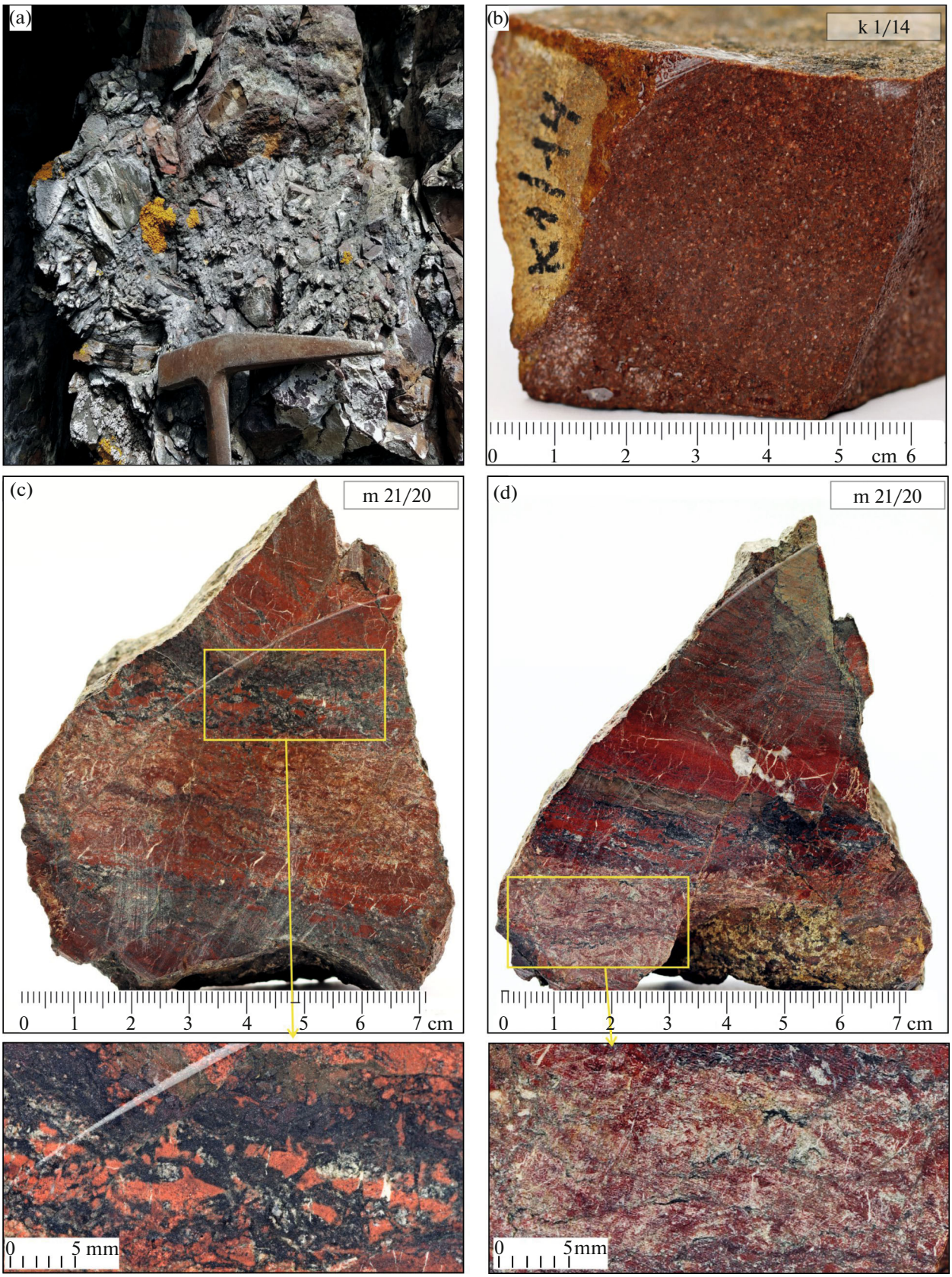

Fig. 4. Samples of the Mara paleovolcano: (a) outcrop of tuff breccias; (b) tuff sandstone used for U–Pb dating of zircon, Sample K1/14; (c, d) intercalation of lilac tuffs and ignimbrites, Sample M21/20. Authors' images.

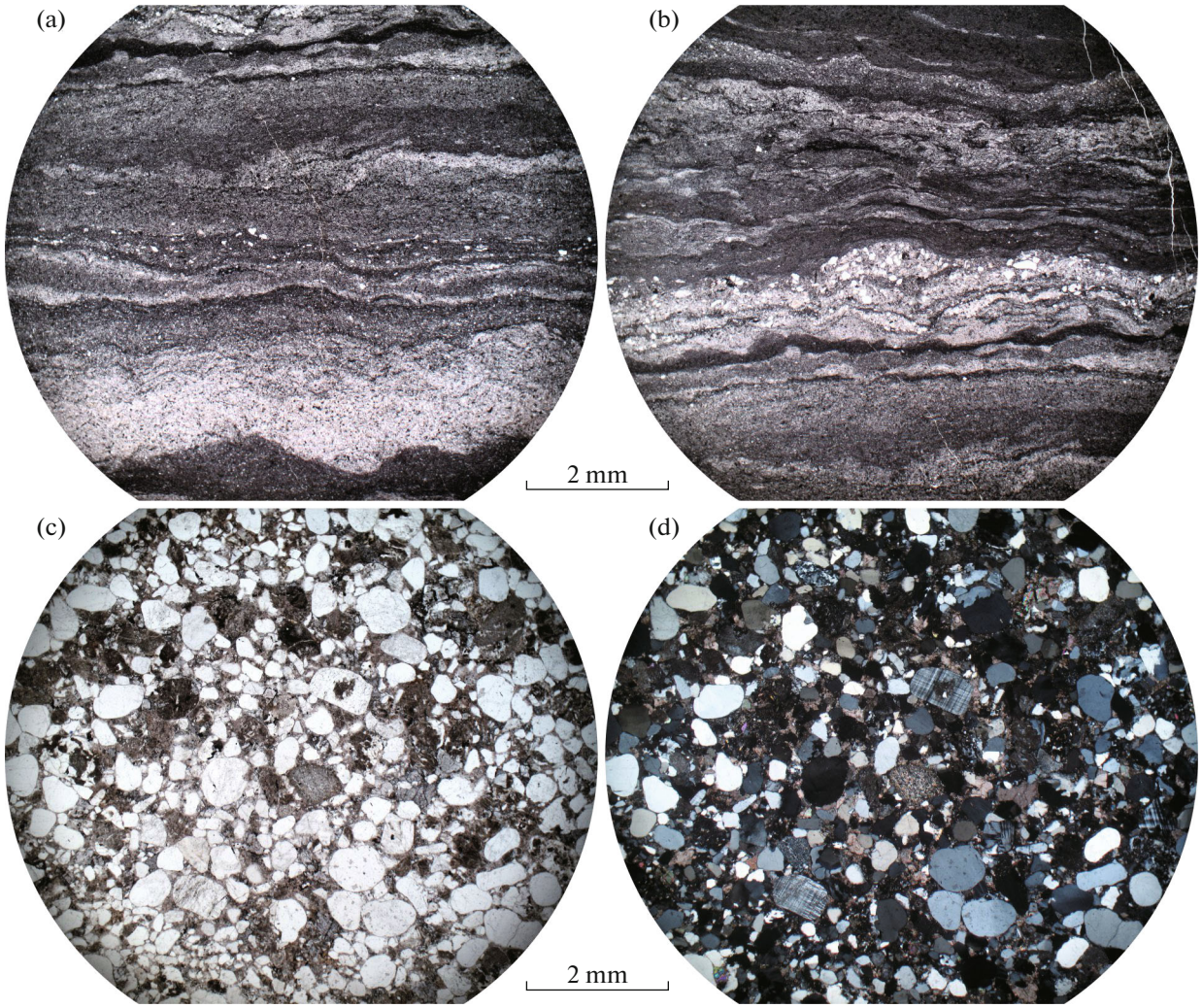

Fig. 5. (a, b) Fine intercalation of vitrocrystal clastic tuffs, tuff siltstones, and sandstones with tuff material (Sample MR15-21), parallel nicols; (c, d) sandstones with volcanic material (Sample MR16-21): (c) parallel nicols; (d) crossed nicols. Thin sections.

ples exhibit the intercalation of bedded and porous tuffs with carbonate matrix. The section is often characterized by fine intercalation of vitrocrystal clastic tuffs and sandstones with tuff material. In tuff interlayers, the crystal clasts are composed of K-feldspar (orthoclase) and acute or angular quartz in contrast to rounded quartz in sandstones. Plagioclase in volcanic rocks is absent. The feldspars in sandstones include microcline and sodic plagioclase and the accessory minerals include tourmaline. These minerals are typical of the basement rocks of the Biryusa Block (Subluk Formation) and granites of the Sayany complex, which underlie the volcano-sedimentary member.

The tuff breccias have a limited occurrence, which is in agreement with the report of (Bessolitsyn et al., 1969). The coarse-bedded unsorted vitrocrystal clastic tuff hosts acute clasts of volcanic rocks (Fig. 6), tuffs, and tuff sandstones of various grain sizes. The volcanic clasts include trachytes and felsites. There are also the fragments of rhyolitic lava breccias with clasts of quartz trachyte. The clast size varies from 0.5 to 5 mm.

The small-grained matrix of the rock is composed of a homogeneous quartz–K-feldspar aggregate with anatase, zircon, monazite, xenotime, and fluorapatite. There are zircon and xenotime intergrowths. Quartz is observed as both small acute unoriented clasts (crystal clasts) and rounded grains. There are also K-feldspar crystal clasts. The matrix is strongly hematitized. Abundant chlorite replaces biotite. In contrast to the phenocrysts, K-feldspar from the groundmass of trachytes has no Ba (Table 2). According to area SEM analysis, the bulk composition of the groundmass corresponds to quartz trachyte. Both phenocrysts and groundmass are totally devoid of plagioclase. There are crystal clasts of clinopyroxene (titanaugite) and titanomagnetite with exsolution structures (ilmenite and ulvöspinel), indicating the presence of mafic rocks in the structure of the volcano.

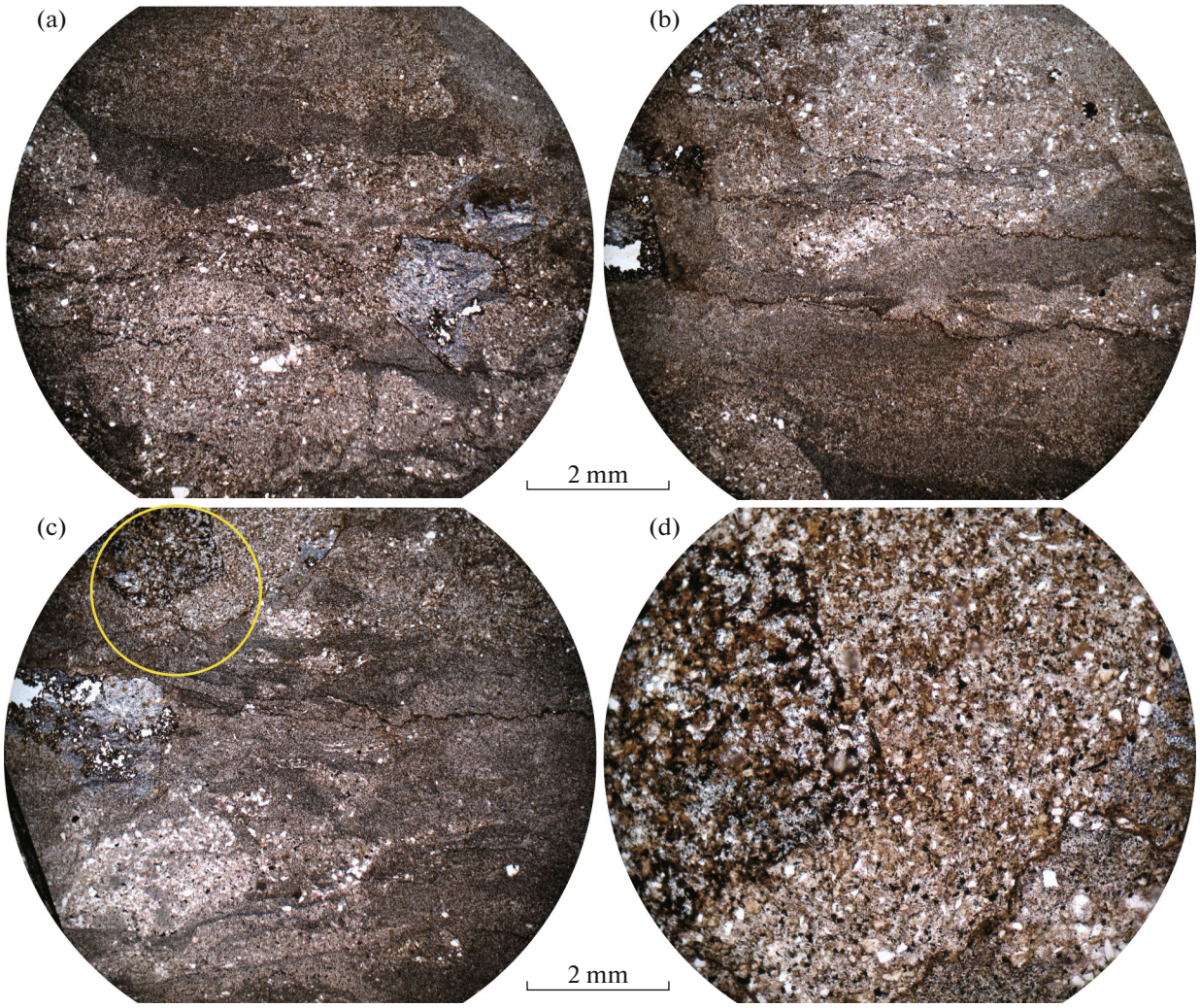

Fig. 6. Tuff breccias with fragments of high-K trachyrhyolites, lava breccias, tuffs, and tuff sandstones (Sample M1-20). Parallel nicols, thin sections.

The coarser grained areas are characterized by the predominance of rounded quartz grains and the presence of microcline, which is atypical of tuff interlayers.

Lithovitrocrystal clastic tuff sandstones with lithoclasts and fiamme of trachytes are most abundant in the section (Fig. 7). The presence of fiamme allows us to consider these rocks as ignimbrites, which were previously described in detail in the region (Fig. 3) (Bessolitsyn et al., 1969). The tuff sandstones exhibit coarse bedding and lack signatures of graded bedding and orientation of quartz and K-feldspar grains. Sample M10/20 contains angular lithoclasts of quenched trachytes (Figs. 7a, 7b), whereas sample M11/20 hosts trachytic fiamme oriented conformably with bedding (Figs. 7c, 7d). This interval also exhibits glassy irregular fragments without sharp contacts with clastic material.

The accessory minerals are the same as in tuff breccias: fluorapatite, monazite, anatase, and zircon, which occur exclusively in K-feldspar groundmass, indicative of high-K volcanism. Some apatite grains are enriched in Sr in the central part. There are zoned zircon crystals, the outer zones of which are rimmed by monazite. Monazite is intergrown with fluorapatite, magnetite, and hematite.

The section contains bedded tuff sandstones with fragments of trachytes, quartz and K-feldspar crystal clasts, and rounded quartz and microcline grains. The lithoclasts include angular fragments of K trachytes (Fig. 8).

The phenocrysts are composed of Ba-enriched K-feldspar laths. There are also angular fragments of altered glass. Quartz is dominant among the clastic material. Perthite-free K-feldspar (orthoclase) and perthite microcline also occur. The accessory minerals include fluorapatite, anatase, zircon, and monazite, as well as tourmaline, which is atypical of volcanic material. Abundant muscovite is also atypical of vol-

Table 2. Chemical composition of minerals (wt %) from volcaniclastic rocks of the Mara volcano

Sample no.	SiO_2	TiO_2	Al_2O_3	FeO_{total}	MnO	Na_2O	K_2O	BaO	V_2O_3	Total
K-feldspar-I										
M5-20	65.34	–	18.42	–	–	–	16.55	–	–	100.31
M8-20	65.19	–	18.37	–	–	–	16.36	–	–	99.91
M23_20	64.67	–	18.48	0.22	–	–	16.55	–	–	99.92
M2_20	64.8	–	18.35	0.6	–	–	16.42	–	–	100.17
M11-20	64.99	–	18.42	0.26	–	–	16.5	–	–	100.18
K-feldspar-II										
M35_20	64.61	–	18.48	–	–	0.51	15.84	0.28	–	99.72
M23_20	64.82	–	18.59	–	–	0.46	16.01	0.33	–	100.22
M23_20	64.89	–	18.57	–	–	0.63	15.52	0.78	–	100.39
M23_20	65.31	–	19.06	–	–	0.2	16.25	1.14	–	101.97
M34_20	63.26	–	18.95	–	–	0.49	15.35	1.33	–	99.37
Anatase										
M1-20	0.22	97.16	0.6	1.11	–	–	1.67	–	–	100.76
M8-20	0.32	99.72	0.47	0.30	–	–	–	–	–	100.81
M11-20	0.56	98.28	0.85	0.71	–	–	0.36	–	–	100.76
M15_20	0.45	99.13	0.28	0.93	–	–	0.16	–	–	100.95
M23_20		99.08	0.68	0.83	–	–	–	–	–	100.59
Magnetite										
M5-20	0.66	0.43	0.36	92.12	0.63	–	0.95	–	0.25	95.40
M11-20	–	0.52	0.89	91.60	0.70	–	0.22	–	0.25	94.18
M30-20	0.36	0.52	0.68	89.84	0.30	–	0.22	–	0.37	92.29
M35_20	0.32	0.35	0.98	92.08	–	–	0.24	–	0.26	94.23
M34_20	0.43	0.27	1.32	90.26	0.45	–	0.84	–	–	93.57
Titanomagnetite										
M1-20	0.98	10.41	1.02	81.95			0.31		0.27	94.94
M1-20	1.99	11.51	0.87	78.49			0.58		0.27	93.71
M1-20	0.48	23.32	0.81	69.29			0.16		–	94.06
Ilmenite										
M1-20	2.12	34.20	0.92	62.33	–	–	0.24	–	0.28	100.09
M1-20	0.51	24.82	0.86	73.73	–	–	0.23	–	0.00	100.14
M1-20	0.34	32.94	0.68	63.00	–	–	0.15	–	0.00	97.10
M1-20	0.56	37.08	0.20	62.38	–	–	-	–	0.00	100.22
M29_20	0.34	46.07	0.00	52.45	0.48	–	0.23	–	0.00	99.58

Dash, the content is below the limit of detection.

canic rocks. The presence of microcline, muscovite, and tourmaline indicate the erosion of rocks of the basement of the volcano.

The tuff sandstones contain thin interlayers of fine-grained tuffs composed of acute quartz and K-feldspar crystal clasts in a fine-grained matrix. Chloritized biotite is abundant. These interlayers are free of graded bedding, sorting, and orientation of crystal clasts.

The section hosts high-K rocks, the K-feldspar groundmass of which contains rhombic dolomite crystals with a high amount of the ankerite end-member (Fig. 9). Similar individuals of zoned dolomite were found in syenites from borehole B-3 of the Bolshaya Taiga pluton, as well as in so-called "sandstones of the Karagas Sequence" (Izokh et al., 2020). In some samples, dolomite and siderite form round grains, which were previously considered a signature of hydrothermal activity of the Mara paleovolcano (Bessolitsyn et al., 1969).

A dolerite dike in the volcano-sedimentary sequence (Fig. 3) was described in (Bessolitsyn et al.,

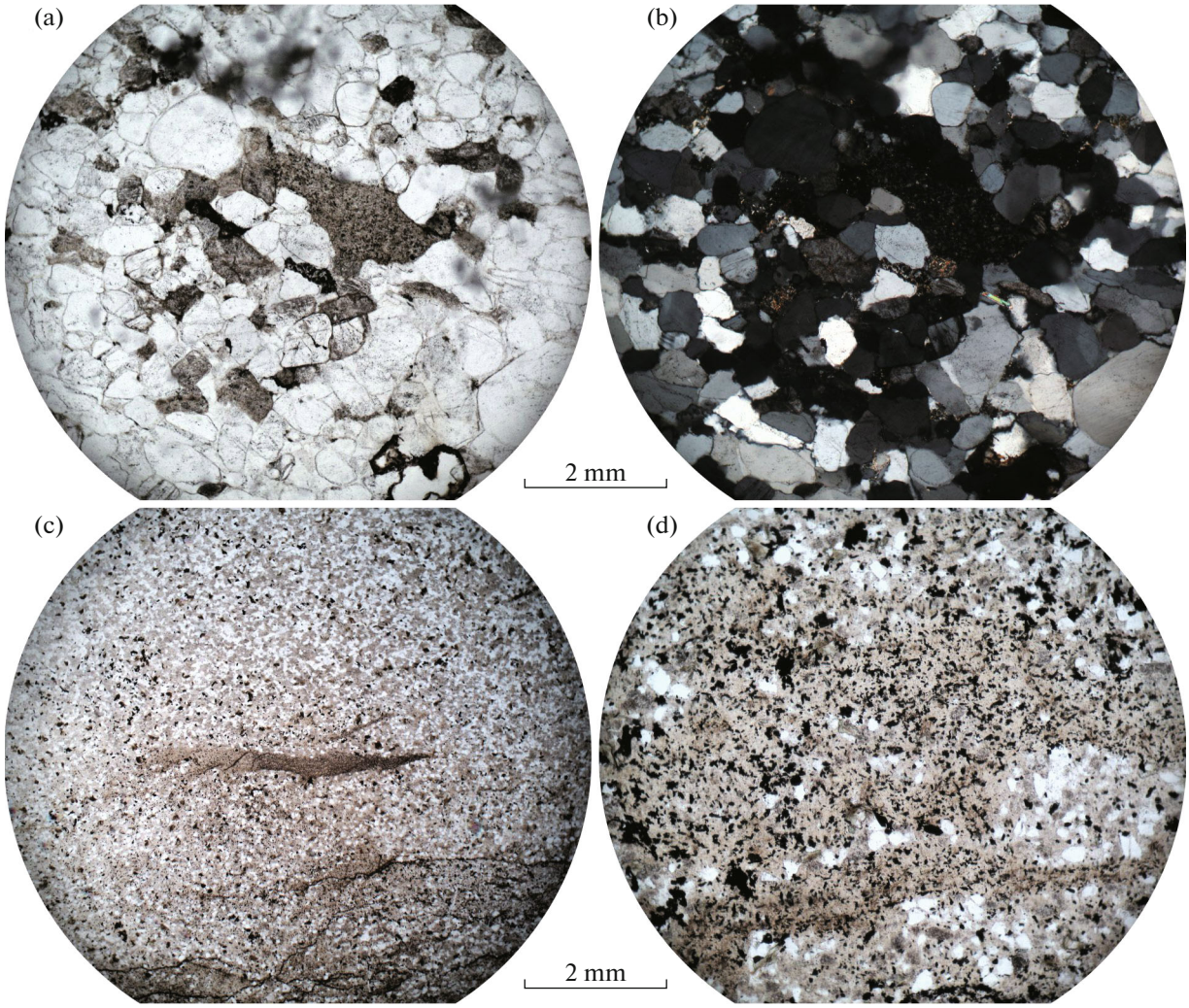

Fig. 7. (a, b) Lithovitrocrystal clastic tuff sandstone with angular trachyte lithoclasts (Sample M10-20): (b) crossed nicols; (c, d) lithovitrocrystal clastic tuff sandstone with trachytic fiamme and lapilli of volcanic glass (Sample M11-20): (d) magnification of 10, parallel nicols. Thin sections.

1969). The authors of the report related this product of mafic magmatism to high-K trachyte–rhyolitic volcanism; however, later these dikes were assigned to the older (780–720 Ma) Nersa complex. We studied this dike made up of well-crystallized trachydolerites with doleritic structure. Clinopyroxene in dolerites includes titanaugite. The major zoned plagioclase is strongly saussuritized. Titanaugite with exsolution structures and apatite are abundant. There are sporadic grains of early chromite. Interstitial quartz–K-feldspar graphics indicates higher K alkalinity of these dolerites. The presence of titanaugite and K-feldspar makes it possible to classify these rocks as K trachydolerites, which distinguishes them from typical tholeiitic dolerites of the Nersa complex. Note that the dikes of trachydolerites cross the volcaniclastic rocks, and at the same time, the tuff material contains clasts of clinopyroxene and titanomagnetite with exsolution structures, which is also indicative of the earlier activity of mafic magmatism.

The presence of tuff breccias with fragments of lavas of trachytes, high-K rhyolits, and basalts and the presence of fiamme of high-K rhyolites and fine-grained vitrolithocrystal clastic tuffs in the studied section thus clearly indicate that they are the fragments of a large Mara paleovolcano (Bessolitsyn et al., 1969). The presence of tuff breccias and signatures of hydrothermal activity (carbonate segregations in tuffs) points to the proximity of the volcano.

MINERALOGICAL PECULIARITIES OF THE VOLCANIC ROCKS

The study of the mineral composition of the Mara volcano showed that most rocks are composed of K-feldspar and quartz with some amount of volcanic glass. The subordinate and accessory minerals include muscovite, chlorite, rutile, magnetite, ilmenite, zircon, apatite, dolomite, and Fe hydroxides. The variations in chemical composition are shown in Tables 2 and 3.

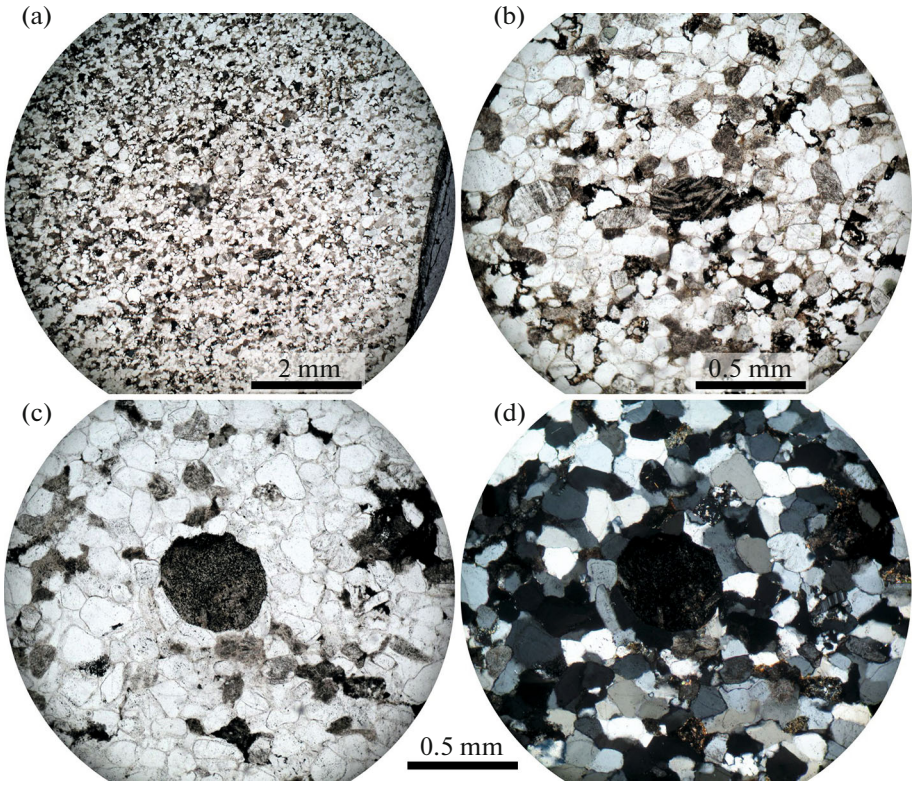

Fig. 8. (a, b) Massive pink lithovitrocrystal clastic tuff sandstone with angular trachyte lithoclasts (Sample M7-20); (c, d) pink lithovitrocrystal clastic tuff sandstone with rounded trachyte lithoclasts (Sample M8-20). Magnification of 2.5 (a) and 10 (b, d); (c) parallel nicols; (d) crossed nicols. Thin sections.

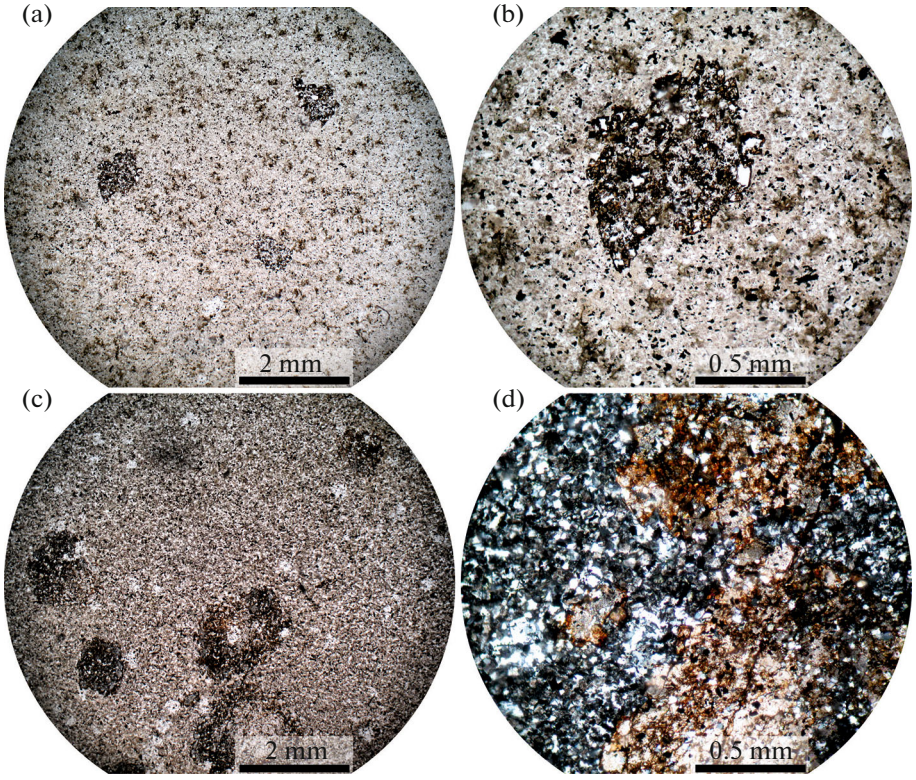

Fig. 9. Fine-grained vitrocrystal clastic tuff with dolomite aggregates: (a, b) Sample M4-20; (c, d) Sample M5-20. Magnification of 2.5 (a, c) and 10 (b, d). Thin sections.

Table 3. Representative chemical compositions of apatite and dolomite (wt %) from volcaniclastic rocks of the Mara volcano

Component	Sample number									
	M5-20	M5-20	M23-20	M30-20	M35-20	M5-20	M5-20	M12-20	M23-20	M23-20
SiO_2	0.21	0.24	0.11	0.05	0.11	0.24	0.28	0.24	–	–
FeO	0.6	0.43	0.21	0.12	0.09	1.93	2.08	0.50	2.97	1.78
MnO	0.02	0.02	0.16	0.04	0.09	0.25	0.18	0.15	0.76	0.32
CaO	56.01	55.03	56.55	55.49	56.62	29.52	29.36	30.8	29.61	29.89
MgO	–	–	–	–	–	20.33	20.31	21.56	19.15	20.13
SrO	0.02	0.02	0.04	0.04	0.03	–	–	–	–	–
Na_2O	0.08	0.26	0.08	0.02	0.08	–	–	–	–	–
Ce_2O_3	0.4	0.33	0.15	0.06	0.05	–	–	–	–	–
La_2O_3	0.25	0.18	0.03	0.03	0.02	–	–	–	–	–
Nd_2O_3	0.09	0.1	0.09	–	0.06	–	–	–	–	–
P_2O_5	40.75	40.22	39.91	41.75	41.47	–	–	–	–	–
SO_3	0.1	0.33	0.03	0.01	0.07	–	–	–	–	–
F	4.01	4.06	4.17	4.76	3.87	–	–	–	–	–
O=F	1.69	1.71	1.76	2.00	1.63	–	–	–	–	–
Total	99.39	98.18	98.64	99.4	100.03	52.27	52.21	53.25	52.49	52.12

Two types of K-feldspar are distinguished on the basis of crystal morphology, texture, and mineral assemblages in the rock (Fig. 10). K-feldspar I forms intergrowths with quartz in the groundmass and contains no Na or Ba. Quartz occurs as relatively large (0.5 mm) elongated and rarely round grains. K-feldspar II forms subhedral and, locally, tabular crystals (phenocrysts) (Fig. 10a). It contains varying BaO (0.3–1.7 wt %) and Na_2O (up to 0.5 wt %) contents. Magnetite is omnipresent (Fig. 10). It forms two evident generations: without exsolution structures (Mag-I) and massive with exsolution structure of ilmenite (Mag-II) and ulvöspinel (Fig. 10b). Mag-I contains a variable amount of TiO_2 (1.0–5.7 wt %) and up to 1 wt % Al_2O_3, V_2O_3, and MnO. Mag-II belongs to titanomagnetite with 10–22 wt % TiO_2. There are ubiquitous small subhedral prismatic, locally, cavernous crystals of Ti oxide (Figs. 10a, 10e). Its crystal structure was resolved using Raman spectroscopy. The mineral was identified as anatase from the Raman bands at 144, 400, and 515 cm^{-1} (positions of peaks). There is also an additional peak at 637 cm^{-1}. Figure 11a shows that the spectra of the anatase samples (1, 2) from volcanic rocks are consistent with that (3) from the RRUFF database (http://rruff.info).

The SEM analyses (Table 2) showed that, in most cases, the Nb_2O_5 content of anatase is below the limit of detection: it ranges from 0.3–0.5 wt % in four cases, reaching 1.02 wt % in one analysis. The mineral always contains Al_2O_3 (0.28–1.19 wt %) and FeO (0.3–1.92 wt %).

Apatite belongs to fluorapatite (up to 5 wt % F). Its Raman spectrum shows a clear peak at 964 cm^{-1}, which is in agreement with numerous analyses of fluorapatite (e.g., peak 7 in Fig. 11b), and two additional peaks at 512 and 580 cm^{-1}. Apatite has low Na_2O (<0.20 wt %), SO_3 (<0.10 wt %), and MnO (<0.10 wt %) contents and a variable amount of FeO (0.1–0.7 wt %), as well as SrO and Cl up to 0.6 wt %. On the SrO–MnO diagram (Fig. 12), most compositions of apatite correspond to the field of lamprophyres. The total REE content typically ranges from 0.1 to 1.7 wt %. In apatite, some $[PO_4]$ anions are replaced by $[SiO_4]$ up to a SiO_2 content of 3.06 wt %. Some analyses exhibit a deficit of the total. The lack of significant variations in other elements (e.g., Ca or Sr) suggests the replacement of CO_3^{-2} by PO_4^{-3}. Clear CO_2 peaks, however, are absent in the Raman spectra (Fig. 11). In addition to apatite, the volcanic rocks contain typical monazite-(Ce). It forms a small dissemination in K-feldspar of both the groundmass and the phenocrysts (K-feldspar II). The grain size varies from 10 to 70 μm.

The zircon morphology in volcanic rocks differs. The dominant grains are irregular with a complex inner structure up to metamictic; euhedral crystals with a homogeneous inner structure are rare. All zircon grains contain a higher amount of HfO_2 (0.9–1.7 wt %). Zircon locally occurs in a close assemblage with xenotime and anatase and xenotime rims zircon (Fig. 10d). The higher Y content in some cases is most likely caused by xenotime microinclusions.

Carbonates occur unevenly in rocks. They include ferroan dolomite (0.2–3.3 wt % FeO) and are observed as both individual aggregates and well-formed crystals (Fig. 10f); they also fill interstices between K-feldspar I

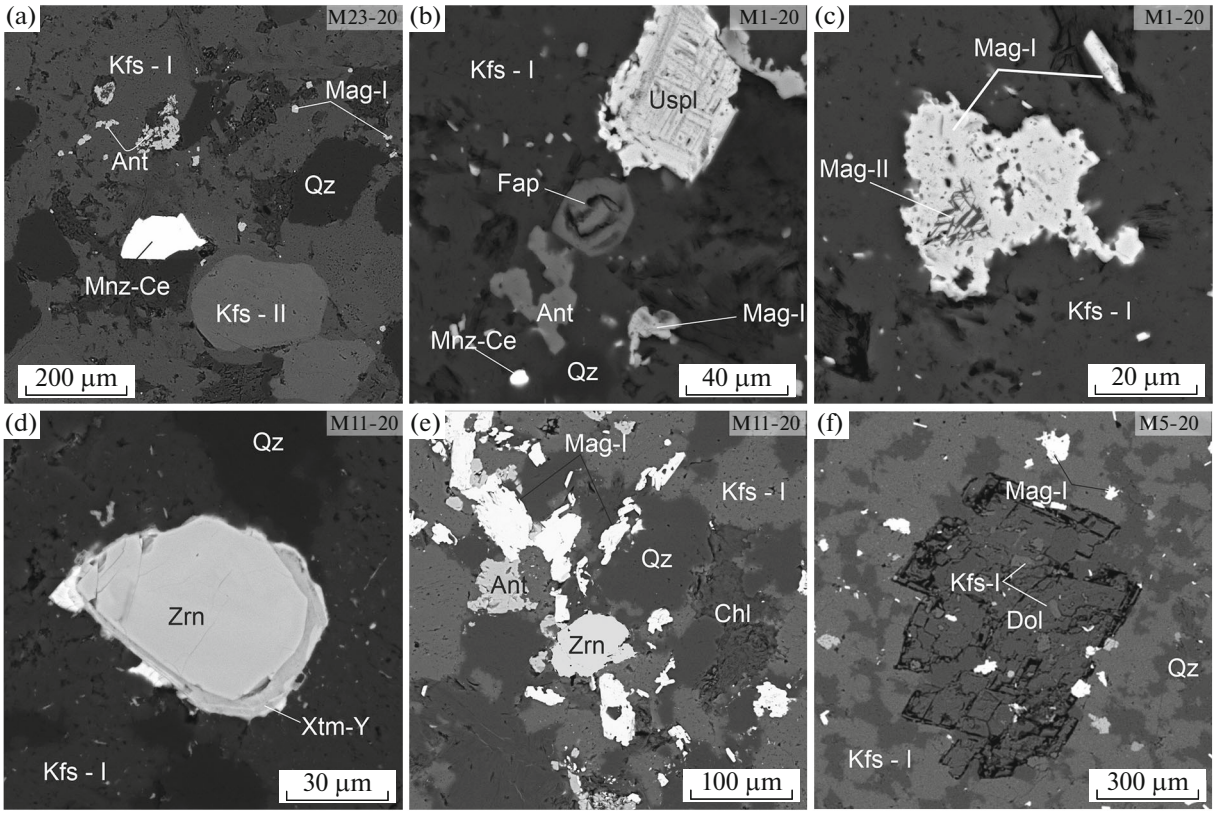

Fig. 10. Peculiarities of structure and interrelations of minerals in rocks of the Mara paleovolcano (BSE images). Symbols of minerals after (Warr, 2021): Ant, anatase; Fap, fluorapatite; Chl, chlorite; Dol, dolomite; Kfs-I, K-feldspar of the groundmass; Kfs-II, K-feldspar phenocrysts; Mag-I, magnetite; Mag-II, magnetite with exsolution structures of ilmenite; Mnz-Ce, monazite; Qz, quartz; Uspl, ulvöspinel; Xtm-Y, xenotime; Zrn, zircon.

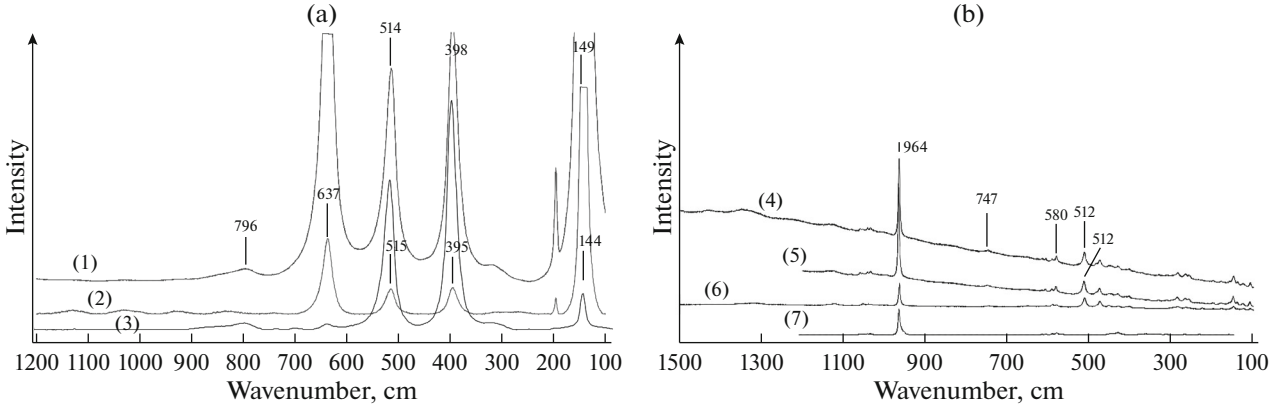

Fig. 11. (a, b) Representative Raman spectra of anatase (spectra 1 and 2) and fluorapatite (spectra 4–6) from rocks of the Mara paleovolcano. The Raman spectra of anatase (3) and fluorapatite (7) are taken from the RRUFF database (http://rruff.info).

and quartz. They host inclusions of magnetite, K-feldspar, rutile, and quartz (Fig. 10f).

GEOCHRONOLOGICAL DATA

The age of volcanomictic high-K rocks in area of the Uvat River (54°50′48″ N, 98°44′31″ E) is estimated on the basis of U–Th–Pb dating of zircon (Table 4). We studied 95 zircon grains and 5 of them are characterized by discordance of >5% and were excluded from further consideration. The most ancient zircon grains have Archean and Paleoproterozoic age (Fig. 13a). A small population includes Neoproterozoic zircon grains (~720 Ma). The age of the main zircon population (>40 grains) is estimated in a range of 630–650 Ma and the average weighted age value by the $^{206}Pb/^{238}U$ isotope ratio is 640 Ma (Fig. 13b). The grains of this population have oscillatory zonation (Fig. 13a).

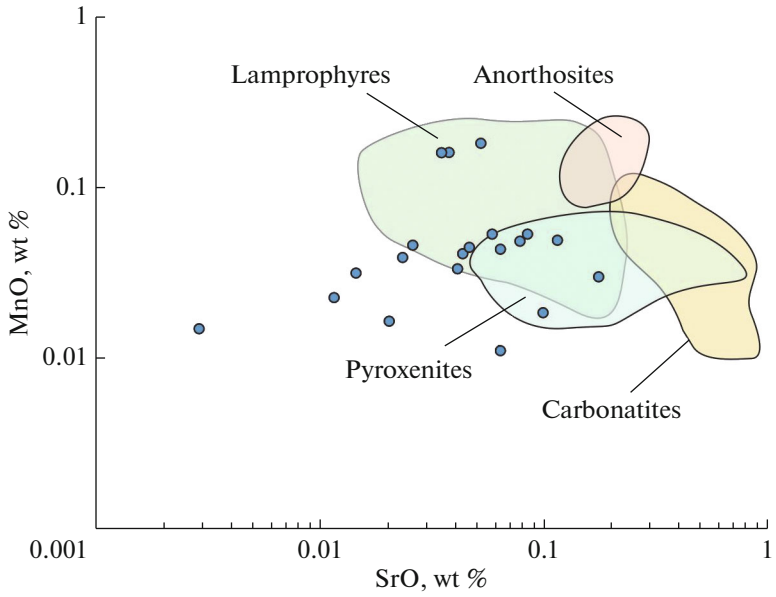

Fig. 12. SrO–MnO correlation in apatite of igneous rocks, composed using materials from GEOROC database (http://georoc.mpch-mainz.gwdg.de/georoc/).

DISCUSSION

Field, mineralogical–petrographic, isotopic–geochemical, and isotopic–geochronological studies of high-K rocks of the Mara–Kamenka–Uvat interfluve showed that they formed as a result of a pulse of explosive volcanism synchronous with alkaline magmatism of the Zima complex (640 Ma) and their referral to the Karagas Group is unwarranted. This area contains felsic ignimbrites, tuff breccias, tuffs, and tuffites, which are intercalated with tuff sandstones and tuff siltstones. The volcanic rocks have a higher K_2O (5–14 wt %) and low Na_2O content. A typical feature of these rocks includes the cherry–lilac, reddish, and pink color, which is caused by abundant superimposed hematitization and a high amount of K-feldspar. The high degree of oxidation of rocks, the presence of ignimbrites and tuffs in the section, and the syneresis cracks indicate the continental volcanism. The high-K rocks in one of the studied primary outcrops have no contact with sedimentary rocks of the Karagas Group and represent individual often elongated isolated fragments of red sequences. They exhibit the intercalation of clastic small- to coarse-grained rocks with massive to bedded textures. Gravel tuff breccias are ubiquitous and contain clasts of altered volcanic rocks. The presence of rounded quartz, microcline, sodic plagioclase, muscovite, and tourmaline indicates the contribution of the basement rocks of the volcano.

The Mara volcanic field hosts abundant bedded tuffs and tuffites with rare interlayers of ignimbrites and tuff breccias. The volcanic rocks correspond to felsic trachytes and trachyrhyolties. No basaltic flows have been identified. The trachybasalts are abundant in the Kremenshet paleovolcano located in this region. At the same time, the tuff material contains clasts of basalts, clinopyroxene (titanaugite), and titanomagnetite with exsolution structures, indicating also the earlier manifestation of trachybasaltic magmatism. The trachydoleritic dikes in the volcaniclastic rocks are mapped in the section of the Mara paleovolcano. The peculiarities of petrographic composition of trachydolerites (the composition of clinopyroxene (titanaugite), quartz–K-feldspar graphics, and the presence of biotite) contradict their link with the tholeiitic dolerites of the Nersa complex (Gladkochub et al., 2012). Similar interrelations of trachybasaltic, trachytic, and high-K rhyolitic magmatism are described in the Permian–Triassic Semeitau volcano-plutonic caldera structure of East Kazakhstan related to the Siberian plume (Ermolov and Izokh, 1977; Dobretsov et al., 2010). In the Semeitau structure, the K trachybasalts begin the volcanic section, whereas the trachydoleritic dikes intrude the subvolcanic granite porphyries and occur only within the volcano.

The studied section contains tuff breccias with fragments of lavas of trachytes, high-K rhyolites, and basalts; the presence of ignimbrites and fiamme of high-K rhyolites and fine-grained vitrocrystal clastic tuffs unambiguously indicates that they belong to fragments of the large Mara paleovolcano (Bessolitsyn et al., 1969). The early geological prospecting works describe rocks with leucite; however, we have not found them yet. The presence of tuff breccias, ignimbrites, signatures of hydrothermal activity (round carbonate nodules in tuffs), and trachydoleritic dikes indicates the proximity to the volcano.

The phenocrysts and crystal clasts of volcaniclastic rocks of the Mara paleovolcano are composed of K-feldspar with a higher Ba content (up to 2%),

Table 4. U–Th–Pb isotope data for zircon from high-K pyroclastic of the Mara volcanic field (Sample K1/14)

1	2	3	4	5	6	7	8	9	10	11	12	13	14	15	16
No.	Sample no., point	Isotope ratios						Rho	Age, Ma						D, %
		$^{207}Pb/^{206}Pb$	±1σ	$^{207}Pb/^{235}U$	±1σ	$^{206}Pb/^{238}U$	±1σ		$^{207}Pb/^{206}Pb$	±1σ	$^{207}Pb/^{235}U$	±1σ	$^{206}Pb/^{238}U$	±1σ	
1	K-1-14-01	0.0648	0.0012	1.0175	0.0197	0.1139	0.0015	0.64	767	77	713	20	**695**	**17**	–2.4
2	K-1-14-02	0.1046	0.0014	4.2784	0.0651	0.2966	0.0038	0.67	**1708**	**50**	1689	24	1675	39	–1.9
3	K-1-14-03	0.0600	0.0008	0.8608	0.0124	0.1041	0.0013	0.68	603	55	631	14	**638**	**15**	1.2
4	K-1-14-04	0.0553	0.0029	0.8253	0.0438	0.1083	0.0017	0.56	423	237	611	48	**663**	**19**	8.5
5	K-1-14-05	0.0736	0.0009	1.7423	0.0240	0.1717	0.0022	0.69	**1029**	**47**	1024	17	1021	23	–0.8
6	K-1-14-06	0.0559	0.0014	0.8119	0.0212	0.1053	0.0014	0.61	449	113	603	23	**645**	**16**	6.9
7	K-1-14-07	0.0604	0.0009	0.8741	0.0141	0.1049	0.0013	0.67	618	62	637	15	**643**	**15**	0.8
8	*K-1-14-08*	*0.1073*	*0.0013*	*2.8444*	*0.0394*	*0.1923*	*0.0024*	*0.69*	*1753*	*43*	*1367*	*20*	*1133*	*26*	*–35*
9	K-1-14-09	0.1244	0.0016	6.1911	0.0912	0.609	0.0047	0.69	**2020**	**44**	2003	24	1986	44	–1.7
10	K-1-14-10	0.0623	0.0010	0.9124	0.0162	0.1062	0.0014	0.66	684	68	658	17	**650**	**16**	–1.2
11	K-1-14-11	0.0599	0.0010	0.8646	0.0153	0.1047	0.0014	0.66	600	70	632	16	**641**	**16**	1.5
12	K-1-14-13	0.0630	0.0011	0.9252	0.0177	0.1066	0.0014	0.65	705	75	665	18	**653**	**16**	–1.8
13	K-1-14-14	0.0596	0.0013	0.8590	0.0202	0.1045	0.0014	0.62	589	97	629	21	**641**	**16**	1.8
14	K-1-14-15	0.1041	0.0015	4411	0.0726	0.025	0.0041	0.67	**1698**	**54**	1701	26	1703	40	0.1
15	K-1-14-16	0.0660	0.0026	1.0950	0.0436	0.1205	0.0019	0.58	804	166	751	41	**733**	**21**	–2.6
16	K-1-14-17	0.1687	0.0022	11.8649	0.1790	0.5102	0.0068	0.69	**2544**	**43**	2593	26	2657	57	4.5
17	K-1-14-18	0.2758	0.0034	25.4494	0.715	0.6695	0.0088	0.69	**3338**	**38**	3325	24	3304	67	–1.0
18	K-1-14-19	0.0605	0.0014	0.9020	0.0214	0.1081	0.0015	0.62	622	97	652	22	**661**	**17**	1.5
19	K-1-14-20	0.1028	0.0013	4.0775	0.0622	0.2877	0.0038	0.68	**1675**	**48**	1649	24	1630	37	–2.7
20	K-1-14-21	0.0810	0.0013	2.2086	0.0402	0.1978	0.0027	0.66	**1221**	**64**	1183	24	1163	28	–4.7
21	K-1-14-22	0.0582	0.0016	0.8947	0.0248	0.1116	0.0016	0.61	535	117	648	26	**681**	**18**	5.1
22	K-1-14-23	0.1129	0.0015	4.9075	0.0752	0.154	0.0042	0.69	**1845**	**47**	1803	24	1767	40	–4.3
23	K-1-14-24	0.0647	0.0016	0.9782	0.0256	0.1098	0.0016	0.62	762	106	692	26	**671**	**18**	–3.1
24	K-1-14-25	0.0627	0.0017	1.0509	0.0298	0.1216	0.0018	0.61	697	117	729	29	**739**	**20**	1.4
25	K-1-14-26	0.0586	0.0011	0.8434	0.0177	0.1044	0.0014	0.64	551	85	621	19	**640**	**16**	3.1
26	K-1-14-27	0.0607	0.0014	1.0564	0.0258	0.1263	0.0018	0.62	627	100	732	25	**766**	**20**	4.7
27	K-1-14-28	0.0591	0.0015	0.8916	0.0241	0.1094	0.0016	0.61	570	113	647	25	**669**	**18**	3.4
28	K-1-14-29	0.0604	0.0009	0.8609	0.0150	0.1035	0.0014	0.66	616	67	630	16	**634**	**16**	0.6
29	K-1-14-30	0.0596	0.0012	0.8670	0.0192	0.1055	0.0015	0.63	588	90	634	20	**646**	**17**	2.0
30	*K-1-14-31*	*0.1086*	*0.0013*	*3894*	*0.0477*	*0.2263*	*0.0030*	*0.70*	*1776*	*42*	*1502*	*21*	*1315*	*31*	*–26*
31	K-1-14-32	0.0590	0.0013	0.8692	0.0204	0.1069	0.0015	0.63	565	97	635	21	**654**	**17**	3.1
32	K-1-14-33	0.1130	0.0014	5.4140	0.0790	0.476	0.0046	0.69	**1847**	**44**	1887	24	1923	43	4.1
33	K-1-14-34	0.1112	0.0013	5.2371	0.0758	0.416	0.0045	0.70	**1819**	**43**	1858	23	1894	43	4.1

Table 4. (Contd.)

1	2	3	4	5	6	7	8	9	10	11	12	13	14	15	16
No.	Sample no., point	Isotope ratios						Rho	Age, Ma						D, %
		$^{207}Pb/^{206}Pb$	±1σ	$^{207}Pb/^{235}U$	±1σ	$^{206}Pb/^{238}U$	±1σ		$^{207}Pb/^{206}Pb$	±1σ	$^{207}Pb/^{235}U$	±1σ	$^{206}Pb/^{238}U$	±1σ	
34	K-1-14-35	0.0641	0.0014	1.0829	0.0246	0.1225	0.0017	0.63	746	91	745	23	**744**	**19**	–0.4
35	K-1-14-36	0.0589	0.0010	0.8708	0.0164	0.1072	0.0015	0.65	563	75	636	17	**656**	**17**	3.2
36	K-1-14-37	0.0601	0.0009	0.8505	0.0142	0.1027	0.0014	0.67	606	63	625	15	**630**	**16**	0.8
37	K-1-14-38	0.0592	0.0009	0.8833	0.0157	0.1083	0.0015	0.66	573	69	642	16	**662**	**17**	3.1
38	K-1-14-39	0.0996	0.0016	3.5297	0.0628	0.2569	0.0036	0.67	**1617**	**59**	1533	2	1474	36	–8.7
39	K-1-14-40	0.1058	0.0014	4.5278	0.0713	0.105	0.0042	0.68	**1727**	**49**	1736	25	1743	41	0.9
40	K-1-14-41	0.0599	0.0009	0.8661	0.0145	0.1049	0.0014	0.67	599	64	633	15.	**642**	**16**	1.5
41	K-1-14-42	0.1125	0.0015	5.1110	0.0807	0.296	0.0044	0.68	**1839**	**49**	1838	25	1836	43	–0.2
42	*K-1-14-43*	*0.0945*	*0.0017*	*2.6710*	*0.0512*	*0.2049*	*0.0029*	*0.65*	*1518*	*66*	*1320*	*2*	*1201*	*30*	*–20.9*
43	K-1-14-44	0.0612	0.0013	0.8774	0.0199	0.1040	0.0015	0.63	646	92	639	21	**637**	**17**	–0.1
44	K-1-14-45	0.0586	0.0014	0.8426	0.0213	0.1042	0.0015	0.62	553	106	620	23	**639**	**17**	3
45	K-1-14-46	0.0604	0.0015	0.8642	0.0226	0.1038	0.0015	0.62	617	108	632	24	**636**	**17**	0.7
46	K-1-14-47	0.0575	0.0012	0.8282	0.0180	0.1045	0.0015	0.64	510	89	612	19	**640**	**17**	4.6
47	K-1-14-48	0.0690	0.0013	1.5064	0.0300	0.1584	0.0022	0.65	897	75	933	24	**948**	**24**	1.6
48	K-1-14-49	0.1225	0.0017	6.0723	0.0997	0.596	0.0050	0.68	**1992**	**50**	1986	2	1980	47	–0.6
49	K-1-14-50	0.0672	0.0031	1.0869	0.0503	0.1172	0.0021	0.58	844	192	747	4	**714**	**23**	–4
50	K-1-14-51	0.0684	0.0010	1730	0.0224	0.1455	0.0019	0.67	881	59	877	19	**876**	**21**	–0.2
51	K-1-14-52	0.1132	0.0014	4.8212	0.0698	0.089	0.0041	0.70	**1851**	**43**	1788	23	1735	40	–6.3
52	K-1-14-53	0.0605	0.0009	0.8811	0.0151	0.1057	0.0014	0.67	619	65	641	16	**647**	**16**	1
53	K-1-14-54	0.0603	0.0025	0.8719	0.0357	0.1050	0.0016	0.58	612	175	636	38	**643**	**19**	1
54	K-1-14-55	0.0751	0.0013	1.7809	0.0348	0.1721	0.0024	0.66	**1069**	**71**	1038	25	1023	26	–4.3
55	K-1-14-56	0.0627	0.0010	1.0660	0.0184	0.1233	0.0017	0.67	698	65	736	1	**749**	**19**	1.7
56	K-1-14-57	0.0599	0.0010	0.8107	0.0155	0.0982	0.0013	0.65	599	75	602	1	**603**	**15**	0.1
57	K-1-14-58	0.0594	0.0013	0.8239	0.0190	0.1005	0.0014	0.63	583	95	610	21	**617**	**16**	1.2
58	K-1-14-59	0.0605	0.0010	0.8787	0.0154	0.1054	0.0014	0.66	620	67	640	16	**645**	**16**	0.9
59	K-1-14-60	0.0635	0.0012	0.8850	0.0177	0.1011	0.0014	0.65	725	78	643	18	**620**	**16**	–3.6
60	K-1-14-61	0.0606	0.0020	0.8457	0.0284	0.1013	0.0015	0.59	623	142	622	30	**622**	**17**	–0.1
61	K-1-14-62	0.0612	0.0010	0.8840	0.0157	0.1048	0.0014	0.66	644	68	643	16	**642**	**16**	–0.1
62	K-1-14-63	0.0665	0.0021	0.9220	0.0295	0.1006	0.0015	0.60	821	131	663	30.	**618**	**17**	–6.9
63	K-1-14-64	0.1668	0.0021	10.9048	0.1664	0.4741	0.0064	0.69	**2525**	**43**	2515	26	2501	55	–1
64	K-1-14-65	0.0602	0.0012	0.8710	0.0183	0.1049	0.0015	0.64	611	84	636	19.	**643**	**16**	1
65	K-1-14-66	0.1067	0.0018	4.5128	0.0843	0.068	0.0043	0.66	**1743**	**61**	1733	29	1724	42	–1.1

Table 4. (Contd.)

1	2	3	4	5	6	7	8	9	10	11	12	13	14	15	16
No.	Sample no., point	Isotope ratios						Rho	Age, Ma						D, %
		$^{207}Pb/^{206}Pb$	±1σ	$^{207}Pb/^{235}U$	±1σ	$^{206}Pb/^{238}U$	±1σ		$^{207}Pb/^{206}Pb$	±1σ	$^{207}Pb/^{235}U$	±1σ	$^{206}Pb/^{238}U$	±1σ	
66	K-1-14-67	0.0584	0.0009	0.7522	0.0136	0.0934	0.0013	0.66	544	70	569	15	**575**	**14**	1.1
67	K-1-14-68	0.1101	0.0015	4.6433	0.0734	0.059	0.0041	0.68	**1800**	**49**	1757	25	1720	40	–4.5
68	K-1-14-69	0.0609	0.0012	0.8717	0.0190	0.1039	0.0015	0.64	633	88	636	20	**637**	**16**	0.1
69	K-1-14-70	0.0650	0.0022	0.9116	0.0318	0.1018	0.0016	0.59	773	145	657	33	**624**	**18**	–5
70	K-1-14-71	0.0609	0.0011	0.8766	0.0171	0.1044	0.0014	0.65	635	76	639	18	**640**	**16**	0.2
71	K-1-14-72	0.0629	0.0025	1.0750	0.0436	0.1241	0.0020	0.58	702	171	741	41	**754**	**22**	1.7
72	K-1-14-73	0.0615	0.0009	0.9036	0.0156	0.1065	0.0015	0.67	657	65	653	16	**652**	**17**	–0.2
73	K-1-14-74	0.1173	0.0014	5.6248	0.0821	0.479	0.0047	0.70	**1915**	**42**	1919	24	1924	44	0.5
74	K-1-14-75	0.0641	0.0009	1.1679	0.0194	0.1322	0.0018	0.68	743	60	785	18	**800**	**20**	1.9
75	K-1-14-76	0.0621	0.0010	1.0176	0.0179	0.1188	0.0016	0.67	678	66	712	1	**723**	**18**	1.5
76	K-1-14-77	0.0651	0.0018	1.0706	0.0301	0.1193	0.0018	0.61	776	114	739	29	**726**	**20**	–1.7
77	K-1-14-78	0.0602	0.0009	0.8725	0.0151	0.1052	0.0014	0.67	609	66	637	16	**644**	**16**	1.2
78	K-1-14-79	0.1204	0.0017	5.6289	0.0917	0.391	0.0047	0.69	**1962**	**49**	1920	26	1882	45	–4.1
79	K-1-14-80	0.1131	0.0014	5.1884	0.0775	0.327	0.0045	0.70	**1850**	**44**	1850	24	1851	43	0.1
80	K-1-14-81	0.0593	0.0014	0.8344	0.0209	0.1020	0.0015	0.62	578	103	616	22	**626**	**17**	17
81	*K-1-14-82*	*0.1006*	*0.0016*	*3222*	*0.0596*	*0.2396*	*0.0034*	*0.67*	*1634*	*59*	*1486*	*27*	*1384*	*34*	*–15.3*
82	K-1-14-83	0.0626	0.0022	1.0200	0.0361	0.1181	0.0018	0.59	695	148	714	35	**719**	**21**	0.8
83	K-1-14-84	0.0598	0.0010	0.8521	0.0156	0.1034	0.0014	0.66	595	71	625	17	**634**	**16**	1.4
84	K-1-14-85	0.0602	0.0012	0.8710	0.0185	0.1049	0.0015	0.64	611	85	636	19	**643**	**17**	1.1
85	K-1-14-86	0.1030	0.0018	3.8118	0.0741	0.2684	0.0037	0.65	**1678**	**66**	1595	30	1532	38	–8.7
86	K-1-14-87	0.0692	0.0010	1395	0.0217	0.1405	0.0019	0.68	903	57	863	18	**847**	**21**	–1.8
87	K-1-14-88	0.0633	0.0012	0.8877	0.0184	0.1017	0.0014	0.64	718	81	645	19	**624**	**16**	–3.2
88	K-1-14-89	0.0693	0.0021	1.1327	0.0355	0.1185	0.0018	0.60	908	126	769	33	**721**	**20**	–6.1
89	K-1-14-90	0.1025	0.0017	3.8344	0.0693	0.2714	0.0037	0.66	**1669**	**60**	1600	28	1548	37	–7.2
90	K-1-14-91	0.0597	0.0010	0.9099	0.0169	0.1105	0.0015	0.66	592	72	657	17	**676**	**17**	2.9
91	K-1-14-92	0.1157	0.0016	5.1558	0.0831	0.232	0.0044	0.68	**1890**	**49**	1845	26	1805	42	–4.5
92	K-1-14-93	0.1047	0.0017	4.4603	0.0815	0.091	0.0043	0.66	**1708**	**60**	1723	29	1736	42	1.6
93	K-1-14-94	0.0627	0.0011	1.1107	0.0214	0.1285	0.0018	0.65	697	74	758	20	**779**	**20**	2.8
94	*K-1-14-95*	*0.1027*	*0.0015*	*3.5188*	*0.0604*	*0.2486*	*0.0034*	*0.67*	*1672*	*55*	*1531*	*26*	*1431*	*35*	*–14.4*
95	K-1-14-96	0.0638	0.0012	1.0583	0.0210	0.1203	0.0017	0.65	734	77	733	20	**732**	**19**	–0.1

The age values of <1 Ga and >1 Ga are calculated from $^{206}Pb/^{238}U$ and $^{207}Pb/^{206}Pb$ (bold) ratios, respectively. Data with discordance of >10% are typed in italics. D, %, discordance calculated from formulas $D = ((^{207}Pb/^{235}U/^{206}Pb/^{238}U) - 1) \times 100$ and $D = ((^{207}Pb/^{206}Pb/^{206}Pb/^{238}U) - 1) \times 100$ for rocks of <1 Ga and >1 Ga, respectively. Rho, correlation coefficient between errors of determination of $^{207}Pb/^{235}U$ and $^{206}Pb/^{238}U$ ratios. $Rho = [1\sigma/(^{206}Pb/^{238}U)]/[1\sigma/(^{207}Pb/^{235}U)]$.

(a)

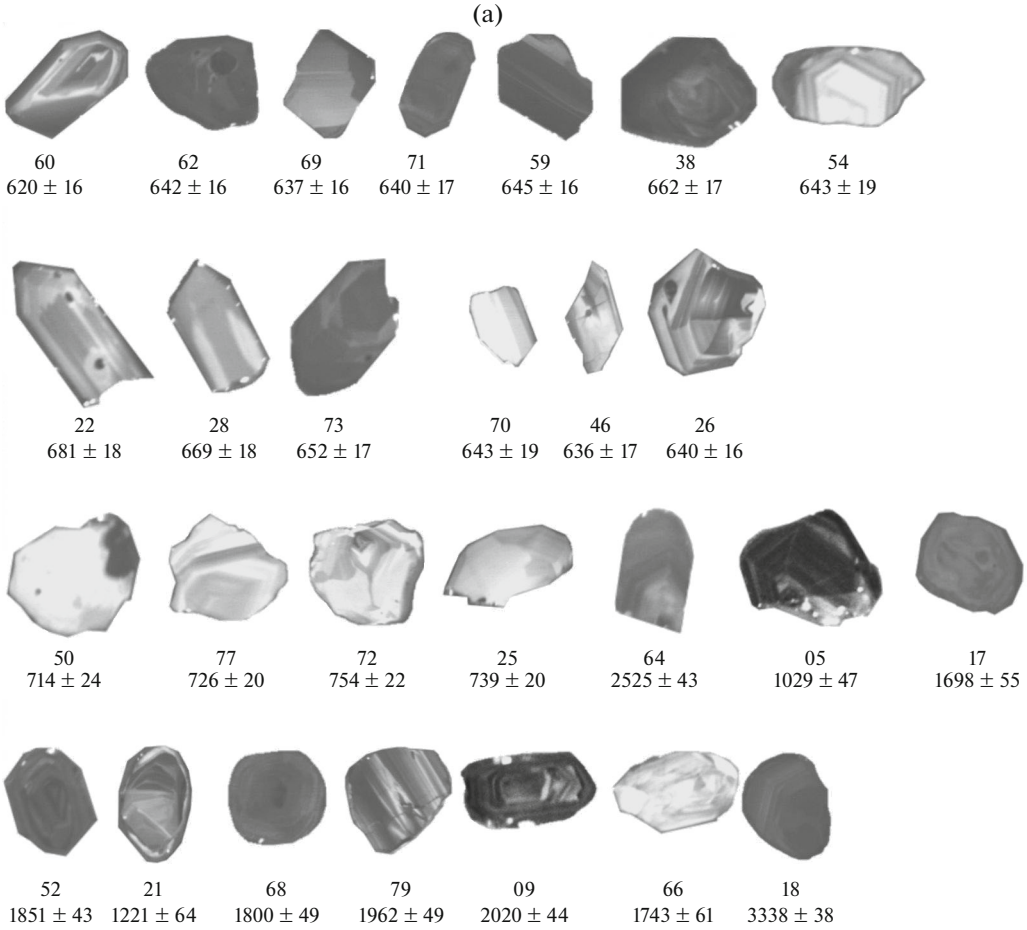
60
620 ± 16
62
642 ± 16
69
637 ± 16
71
640 ± 17
59
645 ± 16
38
662 ± 17
54
643 ± 19
22
681 ± 18
28
669 ± 18
73
652 ± 17
70
643 ± 19
46
636 ± 17
26
640 ± 16
50
714 ± 24
77
726 ± 20
72
754 ± 22
25
739 ± 20
64
2525 ± 43
05
1029 ± 47
17
1698 ± 55
52
1851 ± 43
21
1221 ± 64
68
1800 ± 49
79
1962 ± 49
09
2020 ± 44
66
1743 ± 61
18
3338 ± 38

(b)

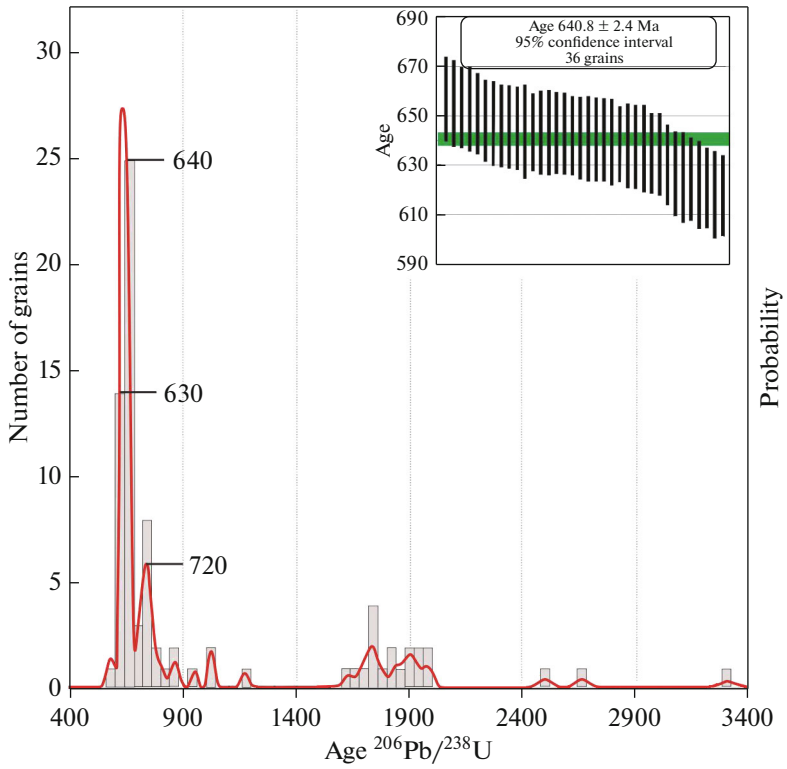
Age 640.8 ± 2.4 Ma
95% confidence interval
36 grains
Age
690
670
650
630
610
590
640
630
720
Number of grains
Probability
Age 206Pb/238U
0
5
10
15
20
25
30
400
900
1400
1900
2400
2900
3400

Fig. 13. (a) Cathodoluminescence images of zircons from volcanomictic high-K rocks (Sample K1-14) with age values (Ma); (b) histogram, plots of probability density of distribution of U–Th–Pb isotopic age of zircon and its average weighted value from volcanomictic high-K rocks (by $^{206}Pb/^{238}U$ ratio, error of 1σ).

whereas K-feldspar in the groundmass contains no Na and Ba. An assemblage of accessory minerals with zircon, monazite, xenotime, anatase, titanomagnetite, and fluorapatite, as well as their composition, is typical of intrusive rocks of the Zima complex. It is likely that the clastic material for the volcano-sedimentary rocks of the Mara field was sourced from rocks similar to the Zima complex. This is supported by the presence of interlayers of rocks with K-feldspar with inclusions of zoned well-faceted dolomite and ankerite crystals. Similar rocks are described in the borehole of the Bolshaya Taiga pluton (Izokh et al., 2020).

It is important to note that zircon is closely associated with xenotime and anatase and xenotime forms the rims around zircon. Similar interrelations of zircon, xenotime, and anatase indicate the link of zircon with alkaline volcanism. The grains of this zircon population have a crystal habit and clear oscillatory zonation, and their weighted average age value is 640 Ma (Fig. 13). The Hf isotopic composition of zircon from high-K rocks of the Biryusa Sayan region is similar to that of zircon from rocks of the Belaya Zima pluton (part of the Zima complex), confirming their common source and indicating the predominance of the material of isotopically moderate depleted mantle (Fig. 14).

It can thus be considered that bimodal high-K volcanism within the Biryusa Uplift of the Siberian Platform occurred at the boundary of 640 Ma. This conclusion is consistent with the occurrence of alkaline magmatism in the south and southwest of the Siberian Craton. The rocks of the Belaya Zima carbonatitic pluton crystallized at 643 ± 4 Ma on the basis of the U–Pb age of zircons from syenites (Yarmolyuk et al., 2005), 645 ± 6 Ma on the basis of the U–Pb age of garnet from ijolites (Salnikova et al., 2019), and 645 ± 6 Ma on the basis of the Ar–Ar age of phlogopite from carbonatite (Doroshkevich et al., 2016). The age of the crystallization of rocks of the Zhidoi complex of 632 ± 2 is based on U–Pb dating of zircon (Yarmolyuk et al., 2005). Egorov et al. (2010) also indicated the intense Late Riphean high-K and alkaline magmatism and volcanism within this territory. Note that, on the basis of U–Pb dating of zircon, the post-Riphean sandstones of the Biryusa Sayan region also have a peak which reflects a significant presence of rocks with the age of 600–650 Ma among the provenances (Glorie et al., 2014; Vasyukova et al., 2019). The broad abundance of this magmatism and volcanism in the south and southwest of the Siberian Craton is related to the breakup of the Rodinia Supercontinent in the Late Precambrian (700–600 Ma). The margin of the separating Siberian Craton during this period (630–650 Ma) was characterized by the formation of ore-bearing carbonatite and ultramafic–mafic igneous complexes, which are considered the derivatives of mantle plumes (Kuzmin and Yarmolyuk, 2014).

A link between the high-K rocks of the Biryusa Sayan region and derivatives of mantle melts is also evident from Lu–Hf isotope data for the population of the Neoproterozoic zircons (Letnikova et al., 2021). The primary ratios of Hf isotopes calculated for 640 Ma in the youngest zircon population from high-K rocks of the Biryusa Sayan region vary from 0.282883 to 0.282591 at $\varepsilon_{Hf}(t)$ from +18 to +2.3, indicating an isotopic heterogeneity. The main group (38 grains) includes zircons with a $^{176}Hf/^{177}Hf$ (I) ratio of 0.282621–0.282883 and a $\varepsilon_{Hf}(t)$ value of +8.8 to +18.0. The primary isotopic Hf ratios of these zircons are close to the parameters of depleted mantle. A minor fraction of zircons (six grains) have a lower $^{176}Hf/^{177}Hf$ (I) ratio of 0.282457–0.282591 at values of $\varepsilon_{Hf}(t)$ of +2.3 to +7.2, indicating the involvement of an isotopically enriched source (probably, crustal material). It is impossible to distinguish the zircons with different isotope data. In this case, we can discuss the isotopically heterogeneous nature of a source of matter during the formation of high-K pyroclastic rocks. The $\varepsilon_{Hf}(t)$ values are similar to those for carbonatites of the Belaya Zima pluton (Fig. 14) (Khromova et al., 2022).

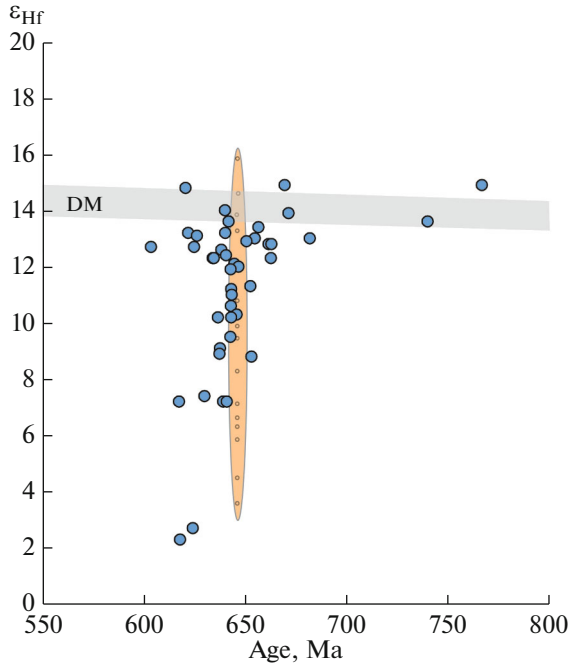

Fig. 14. Age (Ma)–$\varepsilon_{Hf}(t)$ diagram for zircons from high-K pyroclastic rocks of the Mara paleovolcano (blue circles) in comparison with data from carbonatites of the Belaya Zima pluton (orange vertical field) (Khromova et al., 2020). DM, depleted mantle.

The formation of Late Riphean (650–630 Ma) caldera high-K basalt–trachyte–rhyolitic volcanism questions the revision of other sections of the Karagas Group, as well as the volume of the Nersa doleritic complex. The present-day Italian high-K province is the closest analog in peculiarities of high-K volcanism and assemblage of both volcanic and plutonic rocks. A strong Campanian ignimbrite eruption in area of Naples (Italy) occurred at ~40 ka (39 280 ± 110 years ago). It is well studied and is a model object for the estimation of the character of catastrophic eruptions of high-K volcanism. The megaeruption consisted of two phases: Plinian and ignimbrite. According to the volcanic explosivity index, the eruption of the Phlegraean fields was classified 7. The first phase emitted 50 km^3 of solid particles and more than 450 km^3 was erupted to the atmosphere during the second phase. The total volume exceeded 500 km^3. The volcanic emissions slowly precipitated and left a rock apron, which is extended in form of a wedge from South Italy to the northeast to the South Urals. An ash layer covered more than 1.1 million square kilometers, involving the Black Sea region and Caspian Sea. The ash layer reached 1 m on the territory from South Italy to Romania. The volcaniclastic material upon these eruptions thus propagated over vast territories and can be a good indicator and a stratigraphic marker of intraplate high-K magmatism in ancient sedimentary successions.

CONCLUSIONS

The subaerial explosive character of caldera high-K basalt–trachyte–rhyolitic volcanism of the Mara volcano in the Mara–Kamenka–Uvat interfluve of the Biryusa Uplift in the south of the Siberian Platform is substantiated. The mineralogical and petrographic studies indicated a wide occurrence of high-K pyroclastic rocks, ignimbrites, and trachybasalts. The age of high-K volcanic rocks based in U–Th–Pb dating of zircon is 640 Ma. The Lu–Hf isotopic systematics of zircon indicates the relation of this volcanism to mantle magmas. The composition and the time of the formation of the studied rocks is inconsistent with their referral (as was considered before) to the Upper Riphean sedimentary quartz and quartz–feldspar sandstones of the Karagas Group and dolerites of the Nersa intrusive complex. Specific mineralogical–petrographic peculiarities of the studied rocks allow us to use them as a regional stratigraphic marker.

FUNDING

The studies were supported by the Russian Science Foundation: projects no. 19-17-00099 (petrographic, geochronological, and isotopic-geochemical studies) and no. 23-17-00098 (mineralogy of volcanic rocks).

CONFLICT OF INTEREST

The authors of this work declare that they have no conflicts of interest.

Reviewed by A.A. Vorontsov and A.B. Kotov

REFERENCES

van Achterbergh, E., Ryanm, C.G., and Griffin, W.L., GLITTER: On-line interactive data reduction for the laser ablation ICP-MS microprobe, in *Proc. 9th Goldschmidt Conf. Abstract no. 7215*, Cambridge, Massachusetts, 1999.

Bessolitsyn, E.N., Korabel'nikova, V.V., Borisov, V.A., et al., *Margantsenosnost' Severo-Zapadnogo Prisayan'ya. Masshtab 1 : 100 000. Nizhneudinskii, Taishetskii raiony Irkutskoi oblasti. List N-47* (The 1 : 100 000 Map of Manganese Potential of Northwestern Sayan Region, Sheet N-47 (Nizhnyaya Uda and Taishet Disricts of the Irkutsk Oblast)), Irkutsk, 1969 [in Russian].

Dobretsov, N.L., Borisenko, A.S., Izokh, A.E., and Zhmodik, S.M., A thermochemical model of Eurasian Permo-Triassic mantle plumes as a basis for prediction and exploration for Cu–Ni–PGE and rare-metal ore deposits, *Russ. Geol. Geophys.*, 2010, vol. 51. no. 9, pp. 903–924.

Donskaya, T.V., Gladkochub, D.P., Mazukabzov, A.M., and Wingate, M.T.D., Early Proterozoic postcollisional granitoids of the Biryusa block of the Siberian craton, *Russ. Geol. Geophys.*, 2014, vol. 55, no. 7, pp. 812–823.

Doroshkevich, A.G., Izbrodin, I.A., Ripp, G.S., Khromova, E.A., Posokhov, V.F., Veksler, I.V., Travin, A.V., and Vladykin, N.V., Stable isotope composition of minerals in the Belaya Zima plutonic complex, Russia: Implications for the sources of the parental magma and metasomatizing fluids, *J. Asian Earth Sci.*, 2016, vol. 116, pp. 81–96.

Egorov, K.N., Kiselev, A.I., Men'shagin, Yu.V., and Minaeva, Yu.A., Lamproite and kimberlite of the Sayany area: Composition, sources, and diamond potential, *Dokl. Earth Sci.*, 2010, vol. 435, pp. 1670–1675.

Ermolov, P.V. and Izokh, A.E., Petrology of the magmatic rocks of the Semeitau volcanic series, *Geol. Geofiz.*, 1977, no. 6, pp. 52–61.

Gosudarstvennaya geologicheskaya karta Rossiiskoi Federatsii. Tret'e pokolenie. Angaro-Lenskaya seriya, masshtab 1 : 1000000. List N-47 (Nizhneudinsk). Ob"yasnitel'naya zapiska (The 1 : 1000000 State Geological Map of the Russian Federation (3rd ed). Angara-Lena Ser. Sheet N-47 (Nizhneudinsk). Explanatory Note), St. Petersburg: Kart. Fabr. Vseross. Nauchno-Issled. Geol. Inst., 2012 [in Russian].

Gladkochub, D.P., Donskaya, T.V., Ernst, R., Mazukabzov, A.M., Sklyarov, E.V., Pisarevsky, S. A., Wingate, M., and Söderlund, U., Proterozoic basic magmatism of the Siberian Craton: Main stages and their geodynamic interpretation, *Geotectonics*, 2012, vol. 46, no. 4, pp. 273–284.

Glorie, S., De Grave, J., Buslov, M.M., Zhimulev, F.I., and Safonova, I.Yu., Detrital zircon provenance of Early Palaeozoic sediments at the southwestern margin of the Siberian Craton: insights from U–Pb geochronology, *J. Asian Earth Sci.*, 2014, vol. 82, pp. 115–123.

Izokh, A.E., Letnikova, E.F., and Zhmodik, S.M., High-potassium volcanism approximately 640 Ma in the Southwestern Siberian Platform (Biryusa Uplift, Sayan Region),

in *Geodinamicheskaya evolyutsiya litosfery Tsentral'no-Aziatskogo podvizhnogo poyasa (ot okeana k kontinentu). Mater. nauchn. soveshch.* (Proc. Sci. Conf. "Geodynamic Evolution of the Lithosphere of the Central Asian Mobile Belt: From the Ocean to Continent"), Irkutsk, 2020, pp. 133–135.

Khromova, E.A., Doroshkevich A.G., and Izbrodin, I.A., The trace element and Lu–Hf isotope composition of zircons from carbonatites of the Belaya Zima massif (East Sayan), in *Petrologiya i rudonosnost' magmaticheskikh formatsii. Mater. Nauchn. Konf.* (Proc. Sci. Conf. "Petrology and Ore Potential of Magmatic Formations"), Novosibirsk, 2022, pp. 206–209.

Kostitsyn, Yu.A. and Anosova, M.I., U–Pb age of extrusive rocks in the Uxichan caldera, Sredinnyi Range, Kamchatka: Application of laser ablation in dating young zircons, *Geochem Int.*, 2013, vol. 51, pp. 155–163.

Kuzmin, M.I. and Yarmolyuk, V.V., Mantle plumes of Central Asia (Northeast Asia) and their role in forming endogenous deposits, *Russ. Geol. Geophys.*, 2014, vol. 55, no. 2, pp. 120–143.

Letnikova, E.F., Izokh, A.E., Kostitsyn, Yu.A., Letnikov, F.A., Ershova, V.B., Federyagina, E.N., Ivanov, A.V., Nozhkin, A.D., Shkolnik, S.I., and Brodnikova, E.A., High-potassium volcanism approximately 640 Ma in the Southwestern Siberian Platform (Biryusa Uplift, Sayan Region), *Dokl. Earth Sci.*, 2021, vol. 496, no. 1, pp. 53–59.

Metelkin, D.V., *Evolyutsiya struktur Tsentral'noi Azii i rol' sdvigovoi tektoniki po paleomagnitnym dannym* (Evolution of Structures of Central Asia and Role of Shear Tectonics using Paleomagnetic Data), Novosibirsk: Inst. Neftegaz. Geol. Geofiz. Sib. Otd, Ross. Akad. Nauk, 2012 [in Russian].

Romanova, I.V., Vernikovskaya, A.E., Vernikovskii, V.A., Matushkin, N.Yu., and Larionov, A.N., Neoproterozoic alkaline magmatism and associated igneous rocks in the western framing of the Siberian craton: Petrography, geochemistry, and geochronology, *Russ. Geol. Geophys.*, 2012, vol. 53, no. 11, pp. 1176–1196.

Salnikova, E.B., Stifeeva, M.V., Kotov, A.B., Chakhmouradian, A.R., Reguir, E.P., Gritsenko, Y.D., and Nikiforov, A.V., Calcic garnets as a geochronological and petrogenetic tool applicable to a wide variety of rocks, *Lithos*, 2019, vols. 338–339, pp. 141–154.

Savel'eva, V.B., Danilova, Yu.V., Letnikov, F.A., Demonterova, E.I., Yudin, D.S., Bazarova, E.P., Danilov, B.S., and Sharygin, I.S., Age and melt sources of ultramafic dykes and rocks of the Bolshetagninskii alkaline carbonatite massif (Urik-Iya Graben, SW margin of the Siberian Craton), *Dokl. Earth Sci.*, 2022, vol. 505, no. 1, pp. 452–458.

Vasyukova, E.A., Metelkin, D.V., Letnikov, F.A., and Letnikova, E.F., New isotope constraints on the time of formation of the Nersa dolerite complex from the Biryusa–Sayan area, *Dokl. Earth Sci.*, 2019, vol. 485, no. 2, pp. 363–367.

Warr, L.N., IMA–CNMNC approved mineral symbols, *Mineral. Mag.*, 2021, vol. 85, pp. 291–320. https://doi.org/10.1180/mgm.2021.43

Yarmolyuk, V.V., Kovalenko, V.I., Sal'nikova, E.B., Nikiforov, A.V., Kotov, A.B., and Vladykin, N.V., Late Riphean rifting and breakup of Laurasia: Data on geochronological studies of ultramafic alkaline complexes in the southern framing of the Siberian Craton, *Dokl. Earth Sci.*, 2005, vol. 404, no. 7, pp. 1031–1036.

Translated by I. Melekestseva

Publisher's Note. Pleiades Publishing remains neutral with regard to jurisdictional claims in published maps and institutional affiliations.